Colloids and Surfaces A: Physicochemical and Engineering Aspects 733 (2026) 139353

Contents lists available at ScienceDirect

Colloids and Surfaces A: Physicochemical and Engineering Aspects

journal homepage: www.elsevier.com/locate/colsurfa

Sustainable water treatment membranes made with mussel-sourced polydopamine reinforced polymers: Thermo-mechanical characterisation

Güler Türkoğlu Demirkol [a], Kawthr Rukiah [a], İnci Pir [b], Sağra Sağlam [c,*], Mertol Tüfekci [d,e,**], Sevgi Güneş Durak [f], Selva Çavuş [c], Neşe Tüfekci [a]

[a] Faculty of Engineering, Department of Environmental Engineering, Istanbul University-Cerrahpasa, Avcilar, Istanbul 34320, Turkey
[b] Faculty of Mechanical Engineering, Istanbul Technical University, Istanbul 34437, Turkey
[c] Faculty of Engineering, Department of Chemical Engineering, Istanbul University-Cerrahpaşa, Avcilar, İstanbul 34320, Turkey
[d] Centre for Engineering Research, University of Hertfordshire, Hatfield, Hertfordshire AL10 9AB, United Kingdom
[e] School of Physics, Engineering and Computer Science, University of Hertfordshire, Hatfield, Hertfordshire AL10 9AB, United Kingdom
[f] Faculty of Engineering-Architecture, Department of Environmental Engineering, Nevsehir Haci Bektas Veli University, Nevsehir 50300, Turkey

HIGHLIGHTS

- PSf-based ultrafiltration membranes were successfully modified using dopamine and polydopamine.
- PDA coating significantly improved hydrophilicity, mechanical stability, and Mn(II) removal efficiency.
- Tris and dopamine incorporation increased water flux but caused a decline under fouling conditions.
- PVP increased membrane porosity and water retention, enhancing initial filtration performance.
- Membranes containing PSf/PVP/Tris/Dopamine showed the highest pure and lake water flux values.

GRAPHICAL ABSTRACT

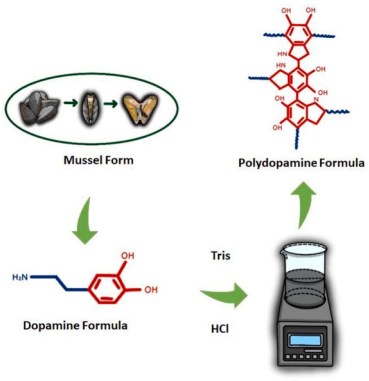

ARTICLE INFO

Keywords:
Sustainable membranes
Mussel-sourced polydopamine
Polysulfone
Characterisation
Mechanical modelling

ABSTRACT

Dopamine, sourced from mussels, was utilised as a sustainable modifier to enhance the thermo-mechanical and filtration performance of polysulfone (PSf)-based ultrafiltration membranes for water treatment. Membranes, fabricated by phase inversion with dopamine/Tris doping (with or without polyvinylpyrrolidone, (PVP)) and polydopamine (PDA) surface coating, were characterised using Scanning Electron Microscopy (SEM), Fourier Transform Infra-red Spectroscopy (FTIR), X-ray Diffraction (XRD), Differential Scanning Calorimetry (DSC), and Dynamic Mechanical Analysis (DMA). Contact angle, water retention capacity (WRC), and porosity were also measured. Micromechanical modelling (Voigt, Reuss, Hill, Self-Consistent) was used to determine the stiffness of the polymers using membrane data. WRC reached 67.6 % for PSf/PVP, decreased to 39.2 % for PSf/Dopamine, and was 63–66.6 % for PDA-coated membranes. Porosity was 15.9–20.2 % for neat PSf and PSf/PVP, reduced to

* Corresponding author.
** Corresponding author at: Centre for Engineering Research, University of Hertfordshire, Hatfield, Hertfordshire AL10 9AB, United Kingdom
E-mail addresses: sagra.saglam@ogr.iuc.edu.tr (S. Sağlam), m.tufekci@herts.ac.uk (M. Tüfekci).

https://doi.org/10.1016/j.colsurfa.2025.139353
Received 9 October 2025; Received in revised form 1 December 2025; Accepted 21 December 2025
Available online 22 December 2025

7.3–8.1 % with dopamine/Tris doping, and increased by PDA coating (17.7–20.9 %). Contact angles of 54–67° indicated increased hydrophilicity with PDA. DSC revealed glass transition temperatures between 201–223 °C, with PVP reducing T_g in a PS-Dopamine system from ~215 °C to ~203 °C. DMA up to 100 °C showed stable storage modulus and rising loss modulus, with higher stiffness in solution-treated membranes than in coated ones. Modelling predicted elastic moduli of polymers in the 180–260 MPa range. Flux performance was highest for PSf/PVP/Tris/Dopamine (487.6 $L{\cdot}m^{-2}{\cdot}h^{-1}$ pure water, 452.5 $L{\cdot}m^{-2}{\cdot}h^{-1}$ lake water, 462.4 $L{\cdot}m^{-2}{\cdot}h^{-1}$ fouled), while Mn(II) removal reached 62 % for PDA-coated PSf/Dopamine. This study presents the first systematic comparison of dopamine/Tris doping and PDA coating, integrating characterisation with modelling and establishes a framework for sustainable membrane design.

1. Introduction

The safe and sustainable supply of drinking water remains one of the most significant global challenges facing humanity today. In response to this pressing issue, continuous advancements in water treatment technologies have become essential. Among these advancements, membrane technology has emerged as a highly effective solution for drinking water treatment. Particularly, composite membranes—created from polymer blends and functional additives—have attracted considerable interest due to their superior performance in water purification and improved mechanical stability [1–3].

Recently, polydopamine (PDA), a biomimetic polymer inspired by the adhesive proteins found in marine mussels, has gained prominence as a versatile material for membrane modification. First introduced by Messersmith in 2007 [4]. PDA is characterised by its robust adhesion properties to diverse surfaces, including metals, ceramics and polymers, attributed to its abundant amino and hydroxyl functional groups [5,6]. Additionally, PDA is notable for its non-toxicity, biocompatibility, and chemical resistance, making it particularly suitable for water treatment applications.

The incorporation of PDA into membrane structures significantly enhances membrane hydrophilicity, antifouling characteristics, and permeability. Hydrophilicity improvements arise from PDA's amine and hydroxyl groups, which strongly interact with water molecules, thereby minimising fouling by reducing contaminant adhesion [7,8]. PDA modifications also improve mechanical and thermal properties, which are necessary as they contribute to the membrane durability and long-term operational stability [9].

Two predominant methods for integrating PDA into membranes are dip-coating and in-situ polymerisation. Dip-coating involves immersing the membrane substrate in a PDA solution, allowing for controlled and uniform deposition of PDA layers on the surface [10]. This method effectively enhances antifouling capabilities by preventing the attachment of contaminants, such as bacteria, proteins, and organic substances, thereby prolonging the membrane's lifespan [11]. It easily and selectively modifies the surface properties. However, it is limited to the surface and may have limited long-term stability due to shallow PDA penetration into the membrane structure.

Alternatively, in-situ polymerisation entails polymerising dopamine directly onto or within the membrane structure during fabrication. This method enables deeper, more uniform incorporation of PDA throughout the membrane matrix, resulting in stronger interfacial adhesion, enhanced mechanical stability, and more durable functional performance. Control over parameters such as dopamine concentration, polymerisation time, and pH enables modulation of membrane pore size, permeability, and selectivity [12]. One promising application involves the integration of PDA with polysulfone (PSf) membranes, which are widely used in water purification due to their desirable mechanical properties. PDA deposition on PSf membranes enhances surface hydrophilicity and antifouling performance without significantly altering the membrane's inherent pore structure, thus preserving filtration efficiency [13,14]. Studies have shown that PDA infiltration into PSf membrane pores slightly reduces pore size while maintaining effective permeation, which is essential for ultrafiltration and advanced osmosis applications [15,16]. However, it is critical to carefully control PDA deposition; excessive PDA loading may lead to pore blockage, thereby negatively impacting water flux and membrane performance [17].

In this study, polysulfone (PSf)-based ultrafiltration membranes were fabricated by phase inversion and modified with dopamine from mussels to enhance sustainability and functionality. Two complementary modification strategies were employed: in-situ polymerisation, enabling bulk incorporation of dopamine into the membrane matrix, and dip-coating, producing surface-level polydopamine (PDA) layers. In addition, polyvinylpyrrolidone (PVP) was introduced as a pore-forming agent to regulate porosity, while tris(hydroxymethyl)aminomethane (Tris) was used to facilitate dopamine polymerisation and stabilise functional group distribution. This systematic framework allowed for the preparation of both neat and modified membranes under identical casting conditions, thereby enabling a controlled comparison between surface and bulk PDA integration routes. Membranes with and without PDA were evaluated in parallel to isolate the effects of dopamine-based modification. At the same time, advanced characterisation techniques were employed to assess morphology, chemistry, thermal stability, hydrophilicity, and mechanical response. These included Scanning Electron Microscopy (SEM), Fourier transform infra-red spectroscopy (FTIR), X-ray diffraction (XRD), contact angle measurements, differential scanning calorimetry (DSC), and dynamic mechanical analysis (DMA). To further interpret the mechanical response, micromechanical homogenisation models (Voigt, Reuss, Hill, and Self-Consistent) were applied to extract the elastic moduli of the polymers from porous membrane data. Membrane performance was also evaluated through water retention capacity, flux, and heavy metal removal efficiency using a dead-end filtration setup.

The novelty of this study lies in presenting the first direct and systematic comparison between PDA dip-coating and in-situ polymerisation strategies within PSf membranes fabricated under identical conditions, while integrating a rigorous experimental programme with micromechanical modelling to assess thermo-mechanical and structural behaviour. This study hence reveals the influence of PDA location and distribution on membrane design and establishes a pathway for sustainable, high-performance water treatment technologies.

The remainder of this paper is organised as follows. Section 2 details the materials, membrane fabrication procedures, and characterisation techniques. Section 3 presents the experimental findings on structural, chemical, thermal, and mechanical behaviour, together with mechanical modelling and performance evaluation. Section 4 concludes the paper with the most important findings and implications for future membrane design.

2. Materials and methods

2.1. Materials

For the fabrication of membranes, PSf (transparent pellets, molecular weight ~35,000 Da) acquired from Sigma-Aldrich was utilised as the primary polymeric material. N-methyl-2-pyrrolidone (NMP) of 99.5 % purity (Emplura®) was selected as the solvent for polymer dissolution. Polyvinylpyrrolidone (PVP, powder form), obtained from Sigma-

Aldrich, served as the pore-forming additive to regulate membrane porosity. Additionally, dopamine and tris(hydroxymethyl)aminomethane (Tris), also supplied by Sigma-Aldrich, were incorporated as functional additives to improve the mechanical, thermal, and surface characteristics of the resultant membranes. All materials were employed without any further purification steps.

2.2. Preparation of neat and composite membranes

2.2.1. Preparation of neat membranes (PSf – PSf/PVP)

PSf membranes were prepared by the phase-inversion method, a technique that relies on the exchange of solvent and non-solvent (water) to induce polymer precipitation. Before membrane preparation, PSf and PVP polymers were dried at 100°C for 24 h in an oven to eliminate residual moisture. The neat PSf membrane casting solution consisted of 15 % PSf and 85 % NMP solvent by weight. For the composite PSf/PVP membrane, the composition was adjusted to 15 % PSf, 5 % PVP, and 80 % NMP.

To prepare the neat PSf solution, 85 g NMP was first transferred to a 250 mL capped bottle placed on a heated magnetic stirrer. The stirring was set at 500 rpm, and the temperature was maintained at 60°C. Subsequently, 15 g of PSf pellets were gradually added to the solvent, and the mixture was stirred continuously for 24 h to ensure complete dissolution and a homogeneous casting solution. For the PSf/PVP composite membrane solution, the preparation method was similar. Initially, 80 g NMP was added to a capped bottle and stirred at 500 rpm and 60 °C. Subsequently, 5 g of PVP was slowly added to the solution. Afterwards, 15 g of PSf pellets were added, and the mixture was continuously stirred under identical conditions for 24 h. After homogeneous solutions were achieved, both solutions were subjected to ultrasonic treatment at room temperature (25 °C) for 30 min to eliminate air bubbles. Membrane casting was performed on a glass plate using a casting knife set to a thickness of 200 μm. The prepared casting solutions were poured onto the glass plate and spread evenly using the casting knife. The glass plate with the polymer solution was immediately immersed in a distilled water bath, initiating the phase inversion process. During this stage, solvent (NMP) from the polymeric film exchanged with water from the bath, causing rapid solidification and formation of the membrane. After complete solidification, membranes detached spontaneously from the glass plate and floated to the surface of the water bath (Fig. 1). They were subsequently collected, extensively rinsed with distilled water to remove residual solvents and impurities and stored at + 4 °C until characterisation.

2.2.2. Preparation of polydopamine (PDA)-modified membranes (PSf/tris/dopamine - PSf/Dopamine)

For the preparation of the PSf/Tris/Dopamine membrane casting solution, the material composition was set as 15 % PSf, 0.1 % Tris, 0.2 % Dopamine, and 84.7 % NMP solvent. Similarly, for the PSf/Dopamine membrane, the composition was adjusted to 15 % PSf, 0.2 % Dopamine, and 84.8 % NMP solvent. The preparation of PSf/Tris/Dopamine and PSf/Dopamine membrane casting solutions was carried out using the same steps described in Section 2.2.1. Table 1 presents the compositions of the prepared membrane casting solutions. The preparation steps of membranes are given and summarised in Fig. 1.

2.2.3. Membrane coating

2.2.3.1. Preparation of polydopamine solution. For the preparation of the PDA solution, 0.25 g of Tris was initially dissolved in 250 mL of distilled

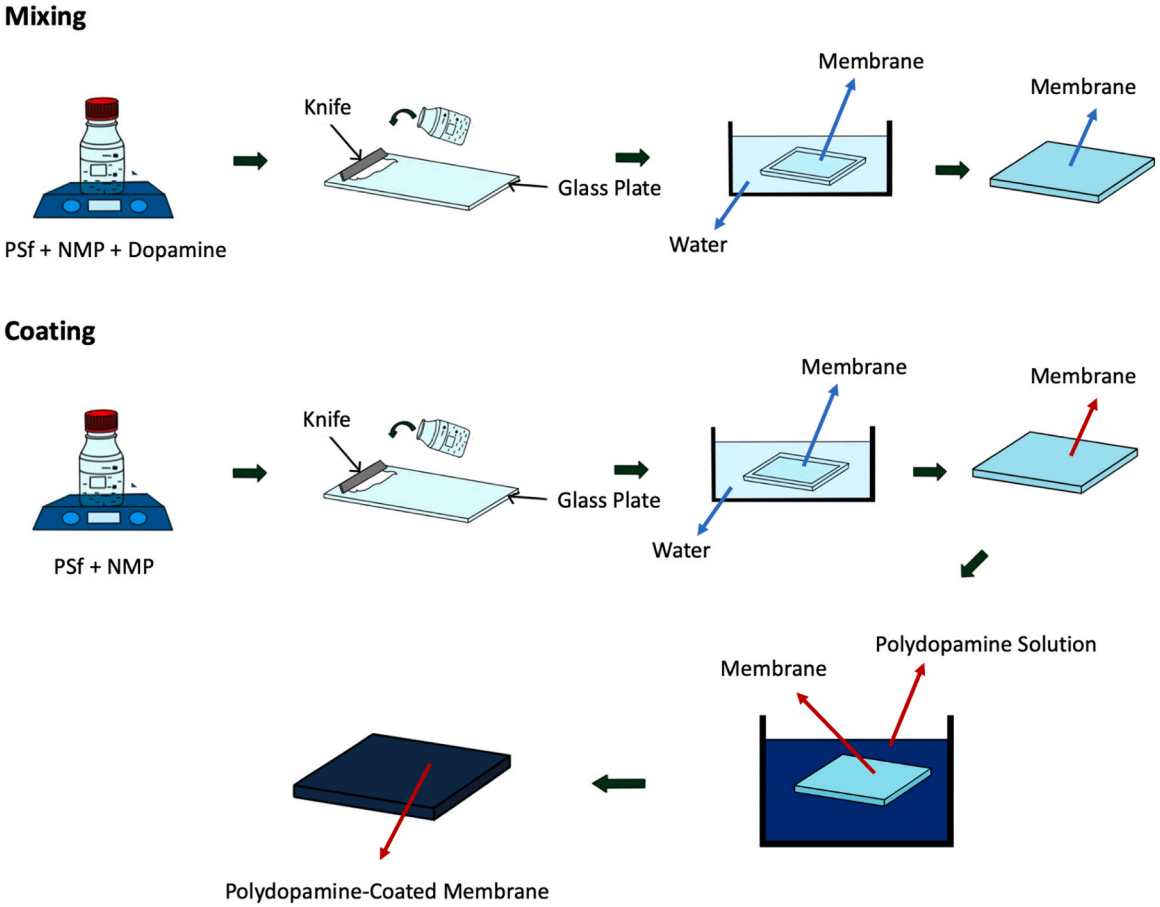

Fig. 1. Schematic illustration of the fabrication steps of PSf and PSf/PVP composite membranes using the phase inversion method.

Table 1
Membrane solution contents.

Membrane Code	PSf (% wt.)	PVP (% wt.)	Tris (% wt.)	Dopamine (% wt.)	NMP
PSf	15	-	-	-	85
PSf -PVP	15	5	-	-	80
PSf/Tris/Dopamine	15	-	0.1	0.2	84.7
PSf/Dopamine	15	-	-	0.2	84.8
PSf/PVP/Tris/Dopamine	15	5	0.1	0.2	79.7
PSf/PVP/Dopamine	15	5	-	0.2	79.8
PSf /PVP (PDA coating)	15	5	-	-	80
PSf/Dopamine (PDA coating)	15	-	-	0.2	84.8

water to form a buffered solution. Since dopamine polymerisation typically occurs under alkaline conditions (approximately pH 8.5), the solution pH was adjusted accordingly before dopamine addition. Subsequently, 0.5 g of dopamine was introduced into the prepared Tris buffer solution. To facilitate dopamine self-polymerisation, the solution was ultrasonicated for 30 min at room temperature. During this polymerisation process, the colour of the solution gradually changed from light yellow to dark brown, indicating the formation of PDA.

2.2.3.2. Coating of prepared membranes with PDA solution. A measured volume of prepared PDA solution was transferred into three separate containers. Subsequently, membranes composed of PSf, PSf/PVP, and PSf/Dopamine, each with a surface area of 96.25 cm^2, were individually immersed in these PDA baths. The coating process was allowed to proceed for 24 h to ensure uniform PDA deposition onto the membrane surfaces. After completing the coating procedure, the membranes were carefully removed and stored in distilled water until further use.

2.3. Membrane surface and morphological characterisation

2.3.1. Scanning electron microscopy (SEM) analysis

SEM is an advanced imaging technique commonly utilised to investigate membrane surface morphology and structure with high spatial resolution. Before SEM analysis, the membrane samples were carefully removed from distilled water and rinsed thoroughly using ethanol-water mixtures to eliminate residual impurities. Subsequently, the washed samples were dried at room temperature. To enhance electrical conductivity and imaging quality, the dried membranes were uniformly coated with a thin gold (Au) layer via sputter coating under controlled voltage and duration parameters. Following the conductive coating process, an SEM analysis was conducted, and high-resolution images of the membrane surfaces were acquired.

2.3.2. Fourier transform infra-red spectroscopy (FTIR)

FTIR is a widely used analytical technique for membrane characterisation. FTIR analysis provides essential information about the chemical composition, functional groups, and molecular structure of membranes. This technique is particularly advantageous as it requires no sample pre-treatment and delivers rapid analytical results. In this study, membrane samples were analysed in the wavelength range of 4000–650 cm^{-1} using a JASCO FT-IR 4700 spectrometer.

2.3.3. XRD analysis

XRD analysis was conducted to determine the crystallographic properties of the membranes using a GNR EXPLORER High Performance Diffractometer (Cu-Ka (1.541874 Å) and 2θ between 2°–90°).

2.3.4. Contact angle

Contact angle measurement is an essential technique for evaluating membrane surface characteristics, particularly their interaction with water. This method reveals the hydrophobic (water-repellent) or hydrophilic (water-attractive) nature of membrane surfaces. Specifically, the contact angle represents the angle formed at the interface where a liquid droplet, typically water, meets a solid surface. A higher contact angle (greater than 90°) indicates hydrophobic behaviour, where the water droplet maintains a more spherical shape due to minimal surface interaction. Conversely, a lower contact angle (typically ranging from 30° to 50°) signifies hydrophilic characteristics, as the water droplet readily spreads across the surface, reflecting stronger interactions. In this study, the hydrophilic or hydrophobic properties of the fabricated membranes were determined using a KSV Instruments CAM 101 contact angle measurement device.

2.3.5. Water retention capacity

Water retention capacity is a critical parameter that quantifies the amount of water retained by membranes. Different approaches may be employed to evaluate this property, depending on membrane type, structure, and application. In this study, membrane samples were prepared by cutting specimens from each membrane type to assess their water retention capacity. Initially, the samples were dried in an oven at 45°C for 48 h, after which their dry weights (W_d) were accurately measured using a precision balance. Following this, dried membrane samples were immersed in distilled water for a predetermined period. Upon completion of this immersion step, the samples were carefully removed from the water bath, gently blotted with absorbent paper to remove excess surface water, and subsequently weighed again to determine the wet weight (W_w). The water retention capacity, expressed as a percentage (%), was calculated using the difference between the wet and dry weights according to Eq. 1:

$$\text{Water Retention Capacity} = \frac{W_w - W_d}{W_w} \quad x \quad 100 \tag{1}$$

2.3.6. Porosity

The porosity of membranes was measured using the wet-dry weight method and calculated using Eq. 2:

$$\text{Porosity} = \frac{(m_w \quad - \quad m_d)}{A\ t\rho} \tag{2}$$

Here, m_w represents the wet weight of the membrane (g), m_d is the dry weight of the membrane (g), A denotes the membrane area (cm^2), t indicates the membrane thickness (cm), and ρ corresponds to the density of water (0.998 g/cm^3).

2.4. Mechanical characterisation of membranes

2.4.1. Dynamic mechanical analysis (DMA)

DMA was conducted to investigate the mechanical properties of the manufactured membranes under ambient conditions. For this analysis, membrane samples previously immersed in distilled water were first dried by storing them at ambient conditions (1 atm, 25 °C) for three days.

DMA measurements can be performed using an analyser equipped with various fixture options. Considering related methodologies reported in the literature [18], the film tension clamp fixture was selected for testing membrane samples. According to the fixture-specific testing guidelines, membrane samples were prepared with dimensions not exceeding 30 mm in length, 7 mm in width, and 5 mm in thickness. In this setup, the upper clamp of the fixture remained fixed while the lower clamp was movable. During the test, mechanical loads were applied via the movable clamp to measure the storage modulus, loss modulus, and tan(δ). The following experimental method, named the Oscillation Temperature Ramp Test (OTRT), involves a controlled, incremental increase in temperature, enabling the continuous monitoring of mechanical property changes. Tests are conducted using a TA Instruments DMA 850.

Before testing, the precise dimensions (width and thickness) of the

membrane samples were measured, and the samples were securely mounted onto the fixture clamps. Following sample mounting, the analyser automatically determined the free length based on the clamp separation distance. Additionally, a preload force of 0.1 N was applied due to the tension clamp configuration. Throughout the DMA tests, a constant strain amplitude of 20 μm was maintained, and the temperature ramp rate was set at 3 °C/min. All measurements were conducted following ASTM D7028–07 standards [19].

2.4.2. Calculation of elasticity moduli of polymers

To complement the dynamic mechanical analysis (DMA) measurements, a micromechanical modelling approach was employed to estimate the intrinsic elastic modulus of the polymer from porous membranes. The membranes were considered as two-phase composites consisting of an isotropic polymer phase and randomly distributed spherical voids representing porosity. The effective modulus measured by DMA corresponds to the porous system, whereas the modelling schemes allow estimation of the intrinsic polymer modulus by accounting for porosity.

Several homogenisation models were used for this purpose, including the Law of Mixtures, the Voigt and Reuss bounds, the Hill average, and the Self-Consistent (SC) scheme. Together, these models provide limiting and intermediate estimates of the effective elastic modulus and, when inverted, enable recovery of the polymer modulus from experimental data.

2.4.2.1. Voigt model (upper bound). The Voigt model assumes uniform strain across all phases, giving an upper bound for the effective modulus as given in Eq. 3:

$$E_V = (1 - \varphi)E_0 + \varphi E_v \tag{3}$$

Here, E_V denotes the effective elasticity modulus predicted by the Voigt model, E_0 is the elasticity modulus of the dense polymer matrix (i.e., without pores), E_v is the modulus of the void phase (assumed ≈ 0), and φ is the porosity volume fraction. This model assumes uniform strain across all phases and provides an upper bound.

For porous systems ($E_v \approx 0$) this simplifies to Eq. 4:

$$E_V = (1 - \varphi)E_0 \tag{4}$$

2.4.2.2. Reuss model (lower bound). The Reuss model assumes uniform stress, providing a lower bound and the mathematical expression is given in Eq. 5:

$$\frac{1}{E_R} = \frac{(1 - \varphi)}{E_0} + \frac{\varphi}{E_v} \tag{5}$$

Here, E_R represents the effective elasticity modulus predicted by the Reuss model. This formulation assumes uniform stress across all phases and therefore provides a lower bound. As E_v approaches zero for voids, the prediction of the Reuss model for porous systems converges to zero.

For porous systems, since $E_v \to 0$ then E_R becomes Eq. 6:

$$E_R \approx 0 \tag{6}$$

2.4.2.3. Hill average. The Hill estimate is defined as the arithmetic mean of the Voigt and Reuss bounds and given in Eq. 7:

$$E_H = \frac{(E_V + E_R)}{2} \tag{7}$$

This midpoint provides a simple approximation that is often closer to experimental behaviour when the material response lies between the uniform stress and uniform strain assumptions.

2.4.2.4. Self-consistent (SC) model. The SC scheme incorporates the interaction between pores and the surrounding polymer through effective medium theory. It considers spherical voids embedded within an effective elastic continuum. The effective bulk modulus K^* of the porous system is obtained as in Eq. 8:

$$K^* = K_m + \frac{[\varphi(K_v - K*)]}{\left[1 + \frac{(K_v - K*)}{\left(K* + \frac{4}{3}G^*\right)}\right]} \tag{8}$$

Here, K_m is the bulk modulus of the dense polymer matrix, K_v is the bulk modulus of the void phase (taken as zero for pores), G^* is the effective shear modulus, which can be calculated as in Eq. 9.

$$G^* = G_m + \frac{[\varphi(G_v - G^*)]}{\left[1 + \frac{(G_v - G^*)}{(G^* + \beta(K^*, G^*))}\right]} \tag{9}$$

Here, G_m is the shear modulus of the dense matrix, and G_v is the shear modulus of the void phase (taken as zero). The correction function β accounts for the influence of spherical inclusions, and the revised expressions given are Eqs. 10 and 11.

$$\beta(K^*, G^*) = \frac{[G^*(9K^* + 8G^*)]}{[6(K^* + 2G^*)]} \tag{10}$$

$$E^* = \frac{9K^*G^*}{(3K^* + G^*)} \tag{11}$$

This model provides a more realistic prediction than the simple Voigt or Reuss bounds, as it captures pore–matrix interactions and their influence on the overall stiffness.

Through these models, the intrinsic polymer modulus can be related to the apparent properties measured in DMA experiments. The Voigt and Reuss formulations provide bounding cases, the Hill average yields a simple intermediate estimate, and the self-consistent scheme leads to a physics-based empirical prediction of the elastic moduli of the polymers that are used to make the porous membranes within the scope of this study.

2.5. Thermal characterisation of membranes

As part of the characterisation studies, the thermal behaviour of the membranes was analysed using a SHIMADZU DSC-60 device. Differential Scanning Calorimetry (DSC) analysis was performed within a temperature range of 25–400 °C at a heating rate of 10 °C/min.

2.6. Flux performance of membranes

The flux test determines how quickly and effectively a membrane allows water to permeate. A dead-end filtration system was used to perform the flux tests of the membranes. The pure water and lake water fluxes of clean membranes, and only the pure water fluxes of fouled membranes, were measured using the dead-end filtration system.

Membrane samples were cut into circular pieces with a diameter of 5 cm and placed at the bottom part of the filtration system. Then, the filtration cell was filled with either pure water or lake water, and both the upper and lower parts were tightly sealed. One end of a hose was connected to a nitrogen gas (N_2) cylinder, and the other end was attached to the top of the filtration cell. Nitrogen gas was used to generate the driving force for water filtration through the membranes.

The permeated water under a pressure of 1.5 bar was collected in a 250 mL beaker placed on a precision balance. The precision balance was connected to a computer via a cable, and the weight values were recorded on the computer over a 10-minute period using the WinCT-RSWeight software in a time–weight format.

As a result, the flux of the membranes was calculated using Eq. 12:

$$J = A^*\Delta t \tag{12}$$

In Eq. 12, J represents the flux (L/m^2.s), V is the volume of the permeate collected (L), A denotes the effective membrane area (m^2), and Δt corresponds to the filtration time (s).

3. Results

3.1. Membrane surface and morphological characterisation

3.1.1. SEM analysis results

SEM surface images of PSf membranes prepared by phase inversion are shown in Fig. 2. When comparing PSf and PSf/PVP membranes, it is observed that the pore structure of the PVP-containing membrane is more pronounced.

The SEM images of PSf and PSf/PVP membranes coated in Tris solution show that, after coating, their pore structures are more distinct compared to uncoated PSf and PSf/PVP membranes. When comparing PSf/Tris/Dopamine and PSf/Dopamine membranes, the pores of the PSf/Dopamine membrane appear more pronounced. Similarly, when comparing PSf/PVP/Tris/Dopamine and PSf/PVP/Dopamine membranes, the pores of the PSf/PVP/Dopamine membrane are more distinct.

This suggests that the Tris additive further reduces pore size, a conclusion supported by porosity experiments. It is considered that the produced membranes fall within the MF-UF membrane size range.

3.1.2. FT-IR results

FT-IR analyses were conducted to examine the structures of the membranes prepared within the scope of the thesis study. The obtained FT-IR spectra are presented in Fig. 3.

The FT-IR spectrum of the membranes prepared in this study exhibits a broad band in the range of 3000–3600 cm^{-1} , which is attributed to O–H stretching vibrations. This observation is consistent with previous reports indicating the presence of catechol and hydroxyl groups in dopamine-containing membranes [17,20–22].

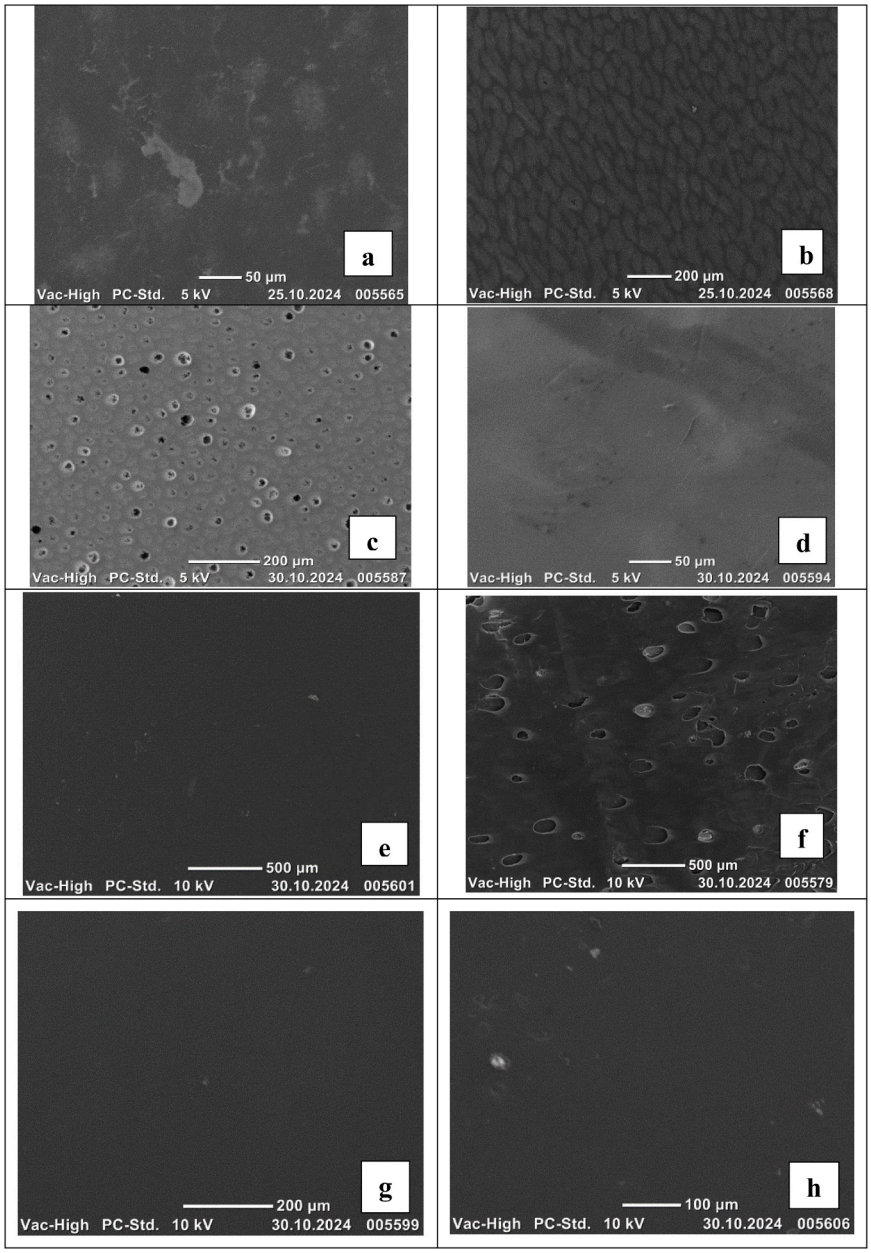

Fig. 2. SEM analysis results (a) PSf, b) PSf/PVP, c) PSf/PVP (PDA coating), d) PSf/Dopamine (PDA coating), e) PSf/Tris/Dopamine, f) PSf/Dopamine, g) PSf/PVP/Tris/Dopamine, h) PSf/PVP/Dopamine).

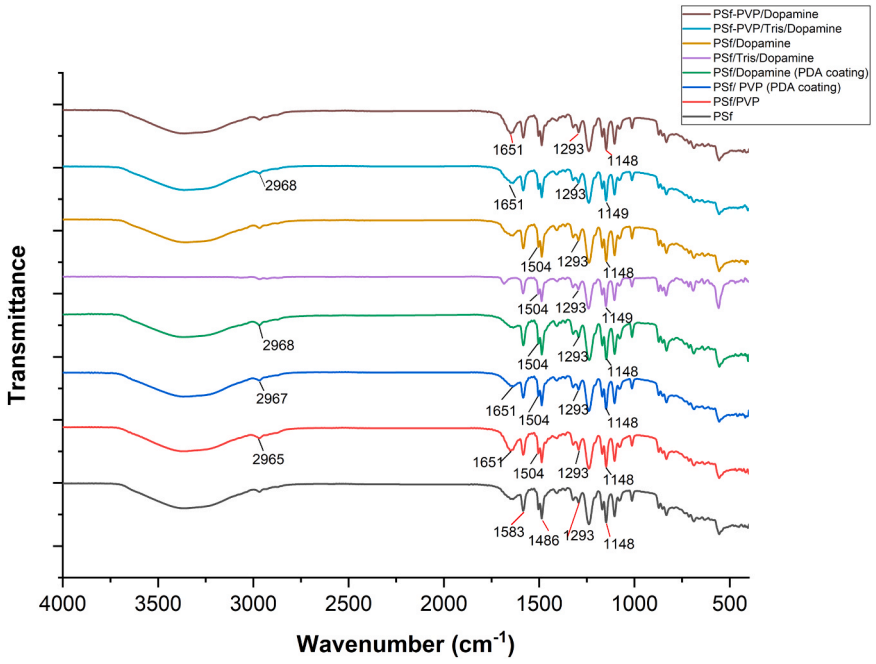

Fig. 3. FTIR analysis results of membrane surfaces.

In the FT-IR spectra of the membranes prepared within the scope of this study, the C–H stretching vibration appears in the range of 2965–2970 cm^{-1} , in agreement with the literature [23–25]. The stretching vibrations of the O═S═O group are typically observed at 1293–1294 cm^{-1} and 1148–1149 cm^{-1} , while the band attributed to the C═C stretching of the aromatic ring is located at approximately 1583–1584 cm^{-1} . These findings are consistent with the characteristic vibrational modes of polysulfone-based membranes as reported in earlier studies [23,26,27].

The peaks observed at 1486 and 1504 cm^{-1} in the FT-IR spectra of membranes containing both PSf and dopamine may also be attributed to the aromatic structures of both components. The peak in the 1293–1294 cm^{-1} can be assigned to C–N stretching, which is also consistent with the presence of dopamine and PVP.

The carbonyl (C═O) stretching vibrations of PVP are observed at 1646 and 1651 cm^{-1} , aligning well with previously reported values for PVP-containing membranes [27–29].

When comparing the FT-IR spectra of PSf-Dopamine and PSf-PVP-Dopamine membranes, the intensity of the peak around 1651 cm^{-1} is found to increase in the presence of PVP, further supporting its successful integration. However, the addition of dopamine to PSf-PVP membranes does not result in a significant spectral shift, which may be attributed to overlapping vibrational bands in the FT-IR region and to the predominance of weak physical interactions, such as hydrogen bonding, rather than the formation of new covalent bonds. Dopamine contains hydroxyl and amine groups that can form hydrogen bonds with both PSf and PVP, but these interactions typically do not cause distinct spectral shifts unless strong chemical bonding occurs. A comparison of the spectra of membranes PSf-PVP and PSf-PVP-Dopamine showed that they were almost similar. Dopamine includes an aromatic ring, a C-N bond and an O-H group in its structure. PSf also has an aromatic ring, and PVP contains a C-N bond. Both the similarity of the bonds and the relatively low amount of dopamine (0.2 %) in the membrane composition, compared to PS (15 %) and PVP (5 %), may lead to overlap. Therefore, the interactions are likely spectroscopically masked in this region for some samples.

Upon addition of Tris base to membranes containing PSf, PVP, and dopamine, an increase in the intensity of the broad band around 3365 cm^{-1} corresponding to O–H and N–H stretching vibrations is observed. This enhancement indicates the presence of additional hydroxyl and amine groups, likely resulting from the dopamine polymerisation facilitated by Tris.

Moreover, in Tris-dopamine-coated membranes containing PSf-PVP, a slight increase is observed in the intensity of the C–H stretching peak at 2967 cm^{-1} , indicating possible interactions between dopamine and polysulfone. Additionally, the intensity of the aromatic C═C stretching peak at 1583–1584 cm^{-1} increases upon the addition of dopamine, suggesting enhanced aromatic character in the membrane matrix.

Furthermore, in membranes prepared with PSf, PVP, dopamine, and Tris base, the peak intensity in the 1635–1651 cm^{-1} range is lower for the coated membranes than for those prepared by other methods. This may be attributed to differences in the extent of dopamine polymerisation or in the interaction between the functional groups during coating, which could affect the vibrational response in this spectral region.

3.1.3. XRD of membranes

The X-ray diffraction (XRD) method is applied for characterisation (spectral) [30] and to clarify the crystalline property of membranes [31]. Muntha et al. (2018) observed that PSf membranes have 2θ values between the range of 18° and 25°regarding the amorphicity [32]. Andrade et al. (2015) fabricated polysulfone-based membranes containing Ag nanoparticles, and the peak 2θ values of 17° and 30° range also show the amorphism of the membrane [33]. XRD patterns of the membranes are given in Fig. 4. In the current study, a broad peak in the XRD pattern of the PSf membrane is seen at 2θ value of 18.90°, indicating the amorphous structure of PSf. However, the strong effect of PVP is clear, and the peak intensity considerably decreases in the XRD pattern of the PSf-PVP membrane, contributing to the increase in amorphous structure compared to the pure PSf membrane. XRD results showed that the presence of PVP contributed to the amorphous structure of the membranes.

3.1.4. Membrane contact angle results

The results of the contact angle measurements revealed that the membranes exhibited contact angles ranging between 54° and 67°, indicating that all membranes possess hydrophilic surfaces. For each membrane type, contact angle measurements were performed three times, and the average values were reported to ensure accuracy and

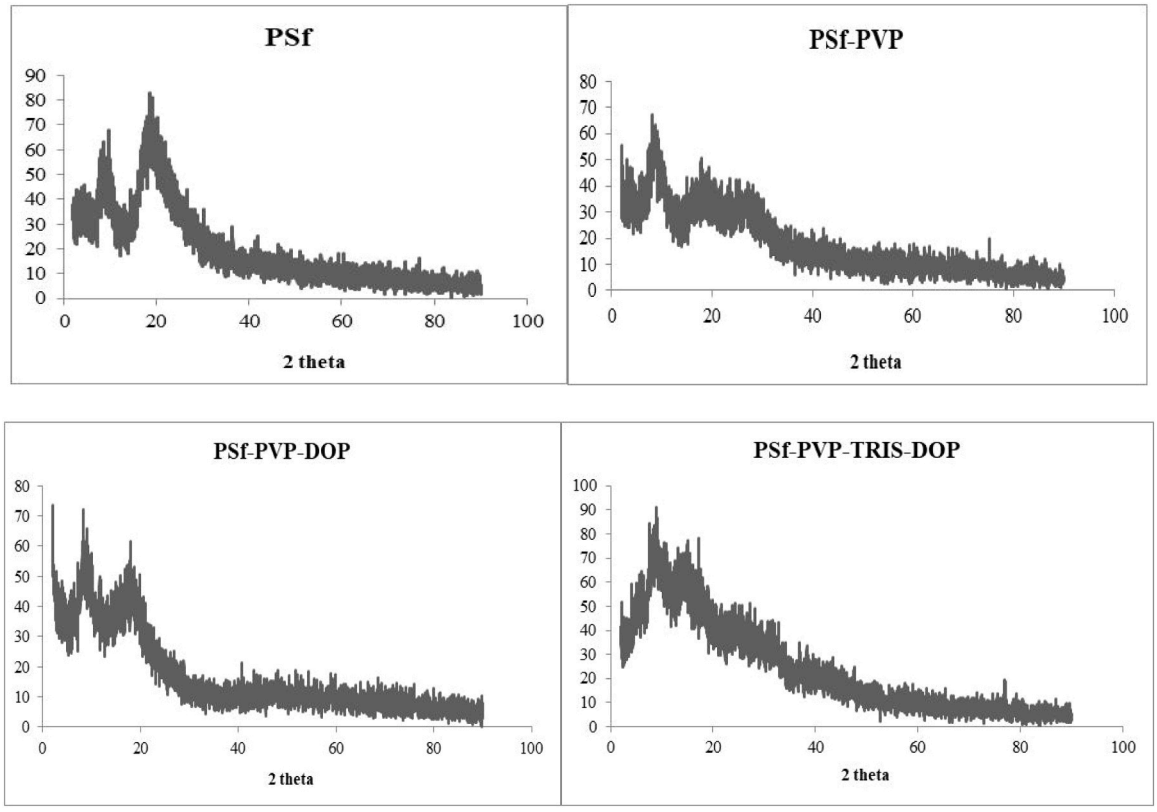

Fig. 4. XRD of the membranes.

reproducibility. PDA-coated membranes showed lower contact angle values compared to both neat and dopamine-doped membranes, suggesting a higher degree of hydrophilicity. Given the inherently hydrophilic nature of PDA-coated surfaces, these membranes are also expected to have an increased water retention capacity. The contact angle values for all membrane types are illustrated in Fig. 5. Compared with the neat PSf membrane, the PDA-coated membrane shows a lower contact angle and greater surface hydrophilicity. Similarly, a slight decrease in contact angle was observed for dopamine- and Tris/dopamine-doped PSf/PVP membranes compared to the neat PSf/PVP membrane, although the reduction was more pronounced in PDA-coated membranes. These findings suggest that both PDA coating and dopamine/Tris doping improve the hydrophilicity of the membranes, likely by introducing hydroxyl (–OH) functional groups. The observed increase in water retention capacity in membranes modified with dopamine and Tris further supports this enhancement in hydrophilicity.

3.1.5. *Water retention capacity results*

According to the analysis results, it was observed that the water retention capacity of dopamine-doped membranes decreased. Among all the membranes tested, the PSf/Dopamine membrane exhibited the lowest water retention capacity, measured at 39.2 %. In contrast, the highest water retention capacity was recorded for the PSf/PVP membrane, reaching 67.6 %. Depending on the membrane composition, the water retention capacity for membranes coated with PDA solution ranged between 63 % and 66.6 %. These variations are illustrated in

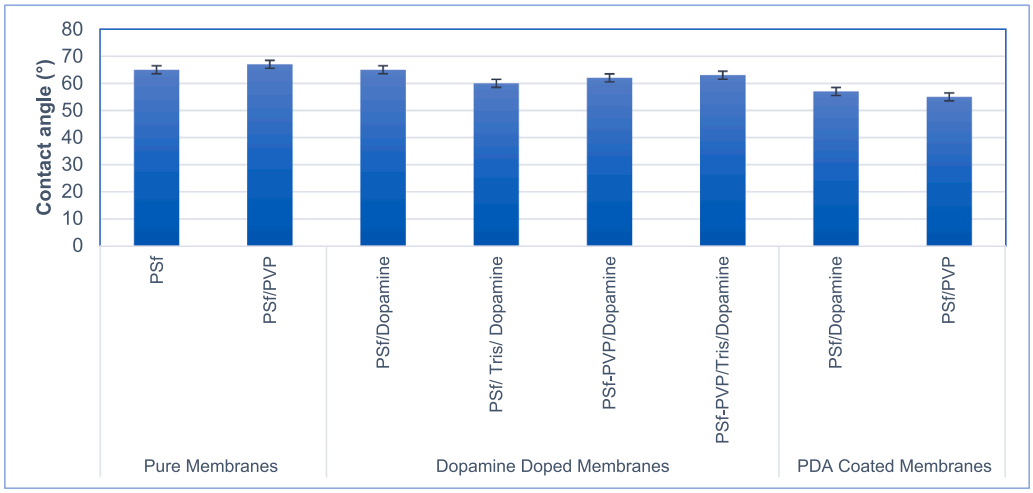

Fig. 5. Contact angle results.

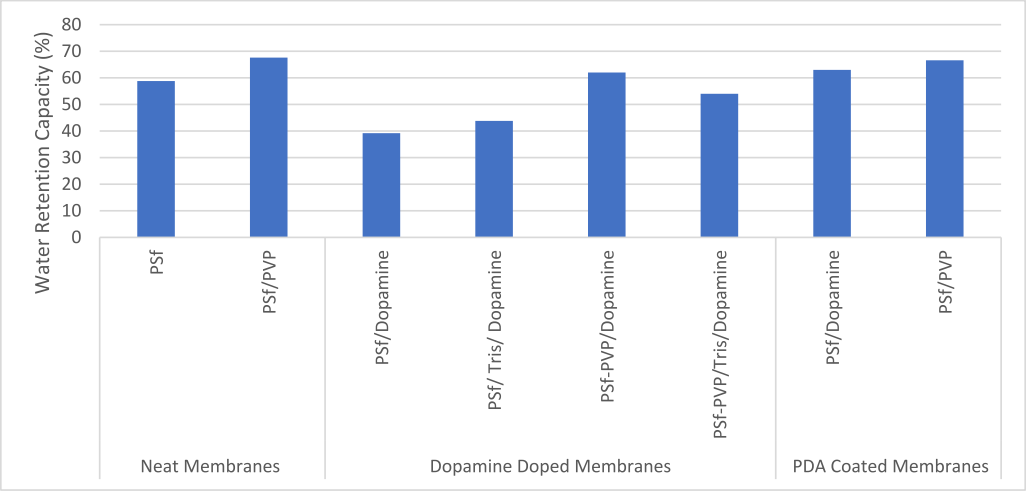

Fig. 6. Water retention capacity results.

Fig. 6.

Following the PDA coating process, a decrease in the water retention capacity of the PSf/PVP membrane was observed, whereas the water retention of the dopamine-doped membrane increased. This suggests that as the dopamine content in PDA-coated membranes increases, water retention capacity also tends to improve. This effect is likely due to the hydrophilic nature of the polydopamine coating, which enhances water affinity on the membrane surface. Furthermore, the presence of Tris during the coating process may help maintain an optimal pH, contributing to a more effective hydrophilic modification. Both dopamine and Tris may increase hydrogen bonding interactions, thereby enhancing the membrane's ability to retain water.

It was also found that dopamine and Tris-dopamine incorporation into neat PSf membranes led to a reduction in water retention capacity. Similarly, doping the PSf/PVP membrane with dopamine and Tris-dopamine resulted in a decrease in water retention. However, it is important to note that PVP, while enhancing pore formation, may also compromise the internal structural integrity of the membrane. As a result, dopamine-doped membranes without PVP exhibited higher water retention compared to their PVP-containing counterparts. These findings are depicted in Fig. 6.

3.1.6. *Membrane porosity results*

Fig. 7 presents the porosity results of the manufactured membranes. The porosity of the neat membranes (PSf and PSf/PVP) ranged from 15.86 % to 20.21 %. In contrast, the porosity of the dopamine-doped membranes was lower, at 7.33 % and 8.08 % for PSf/Dopamine and PSf/Tris/Dopamine, respectively. For membranes containing both PVP and dopamine, the porosity was measured as 17.46 % for PSf-PVP/Dopamine and 12.78 % for PSf-PVP/Tris/Dopamine.

When comparing neat membranes to those modified with dopamine, Tris, and PVP, a noticeable reduction in porosity was observed following the addition of these components. In particular, dopamine and Tris appear to contribute to a denser membrane structure, reducing overall porosity. This effect was especially evident in membranes that originally contained PVP, a typical porosity-enhancing additive. This significant decline in porosity may be attributed to a pore-narrowing mechanism resulting from dopamine-induced changes in membrane morphology. One possible explanation is the interaction between dopamine and the polymer matrix, which may lead to partial pore blockage or wall thickening due to π–π stacking and hydrogen bonding. Additionally, dopamine can undergo oxidative polymerisation, potentially forming crosslinked PDA structures within the membrane, thereby reducing free pore volume. Furthermore, in dopamine/Tris/PVP-containing membranes, the presence of dopamine may interfere with the pore-forming role of PVP during phase inversion. Specifically, dopamine and Tris may hinder the leaching of PVP into the coagulation bath, limiting its ability to create pore channels, and thus suppressing the typical

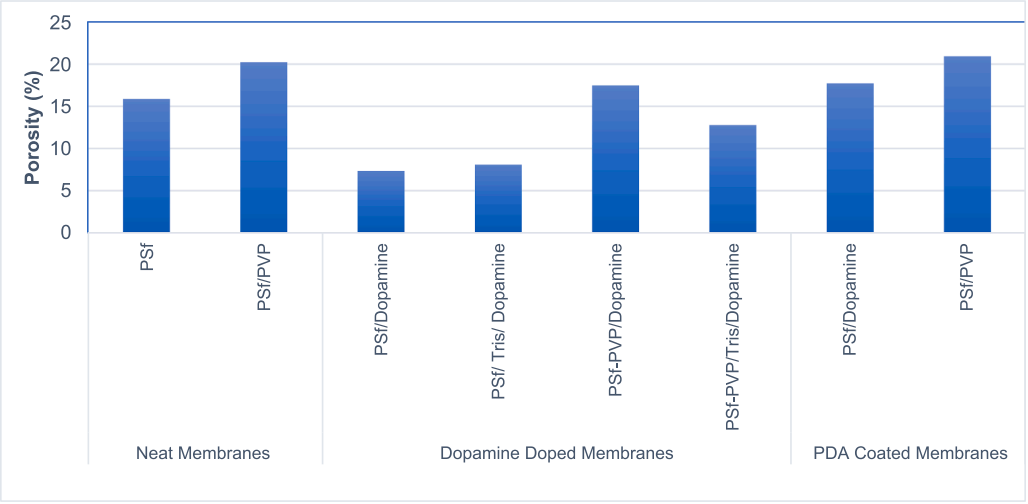

Fig. 7. Membrane porosity results.

porosity-enhancing effect of PVP.

The porosity of PDA-coated membranes was determined to be 20.93 % for PSf/PVP and 17.73 % for PSf/Dopamine. These results indicate that, unlike dopamine and Tris additions, PDA coating did not substantially reduce membrane porosity relative to neat membranes. Therefore, while dopamine and Tris tend to decrease porosity by altering the internal membrane structure, PDA surface coating alone appears to have a minimal impact on overall porosity. The minimal change in overall porosity after PDA surface coating is consistent with previous reports: PDA forms an ultrathin, conformal (and often partially porous/island-like) surface layer that does not fully fill bulk pores unless deposition is extensive, so total porosity remains largely unchanged under the applied coating conditions [34]. However, prolonged deposition or higher dopamine concentrations can increase PDA film thickness and partially block surface pores, reducing permeability and MWCO - a dependence on coating conditions reported in the literature [17,35].

3.2. Mechanical characterisation of membranes

3.2.1. DMA results

The glass transition temperature is the temperature at which a polymer transitions from a glassy, brittle state to a rubbery state [36,37]. It is crucial for determining the thermal and mechanical properties of polymers, influencing their applications and performance [38]. T_g significantly influences the mechanical properties of polymer matrix composite membranes, as it marks the temperature at which the phase change occurs from solid to soft, impacting the viscoelastic properties of the composites [39]. Polyarylene ether ketone (PAEK-COOH) membranes demonstrated a T_g of 220 °C, indicating excellent thermal stability, which is beneficial for high-temperature applications [40]. Reinforcement types also affect the T_g values of composite membranes. Gold nanoparticle reinforcement to poly(styrene-co-chloromethylstyrene) (PSCMS) membranes increased the T_g from 132 °C to 159 °C, showing that nanofillers can significantly enhance the thermal properties of composite membranes [41].

The temperature-dependent mechanical properties test on the membrane samples has been completed, and the storage modulus, loss modulus, and tanδ values have been obtained from the tests. Tests start at ambient conditions, and the temperature is raised by 3 ℃ per minute until it reaches 100 ℃, the boiling point of water. No sharp transition region was observed in the samples with respect to temperature. This indicates that the samples are well below their glass transition temperature and maintain their mechanical stability. As the temperature increases, even though the polymer chains have not yet fully developed their mobility and transitioned to a rubbery phase, the thermal energy imparted to the system increases molecular-level kinetic activity [42]. As temperature increases, local vibrations and rotations of the groups attached to the polymer chain accelerate, increasing intermolecular friction and damping the mechanical energy as heat [43]. Although the material still maintains its macroscopically glassy structure, its loss modulus, characteristic of viscous damping, exhibits a steady increase due to increased thermal activation and molecular friction [44]. The obtained values are presented graphically in Figs. 8–10.

In Fig. 8, the temperature-dependent mechanical behaviour of the PSf membrane is given. When examining the temperature-dependent changes in the mechanical properties of the PSf membrane, it can be interpreted that the storage modulus values of this membrane do not change with temperature. Additionally, the membrane's loss modulus increases with increasing temperature. This suggests that the membrane's behaviour shifts towards a more viscous region as the temperature increases. However, the absence of a sharp decrease also indicates that the material is far from its glass transition temperature.

From Fig. 8, the temperature-dependent mechanical behaviour of the PSf-PVP membrane can be observed. When examining the temperature-dependent mechanical properties of the PVP-doped membrane, the storage modulus follows a nearly linear curve with a slope of nearly zero. In the storage modulus, it is observed that viscous properties become more visible with increasing temperature. The rise in viscous properties indicates an increase in the energy spent on internal friction, as seen in cases such as the loading-unloading of the membrane. Additionally, when the results for PVP-doped membranes are compared with those for PSf membranes, a decrease in the storage modulus is observed. This can be attributed to the pore-forming effect of the PVP, which increases porosity and creates discontinuities in the membrane. For the loss modulus, the results for PSf and PVP-doped membranes are similar at room temperature. However, as the temperature rises, the loss modulus of the PSf membrane increases more rapidly.

Fig. 9 shows the temperature-dependent mechanical behaviour of the PSf-PVP-Tris-Dopamine Coating membrane. PVP-doped membranes were coated with Tris and Dopamine, and the effect of this coating was

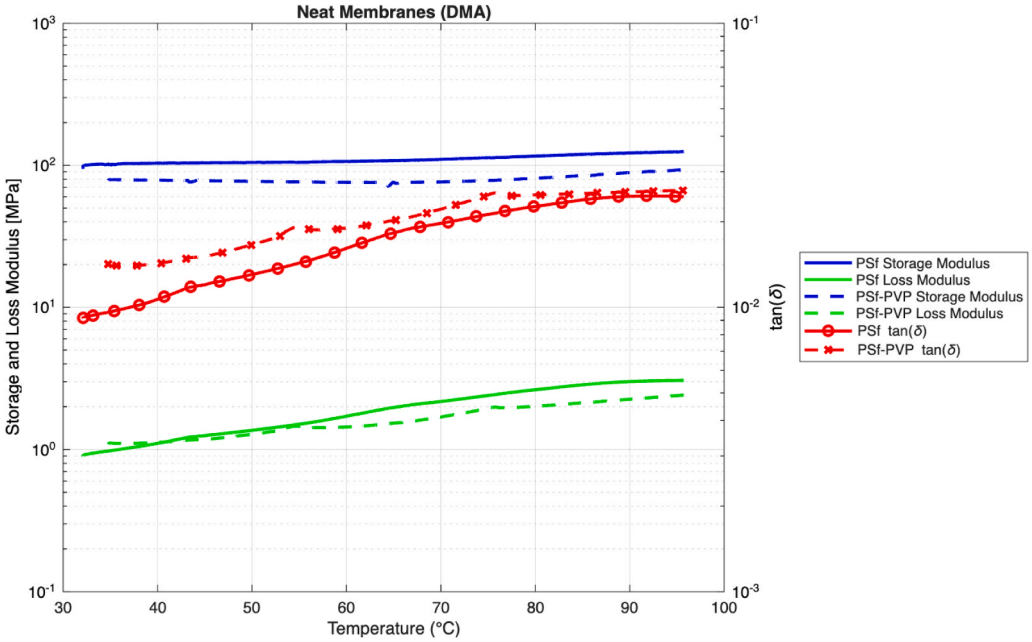

Fig. 8. DMA analysis of PSf and PSf-PVP membranes showing storage modulus, loss modulus, and tan(δ) vs. temperature.

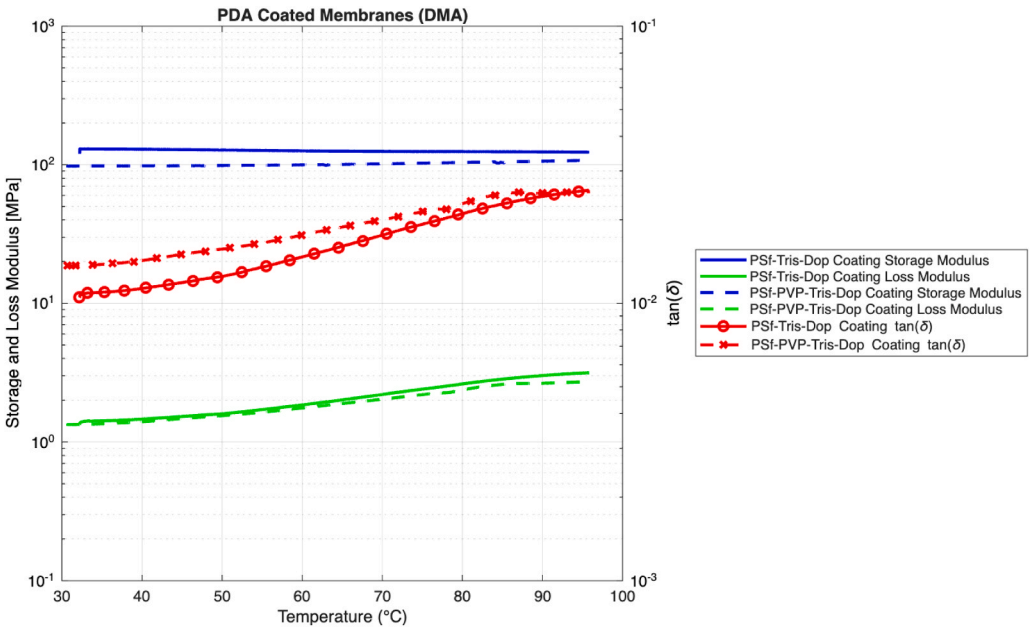

Fig. 9. DMA analysis of PSf-PVP-Tris-Dopamine and PSf-Tris-Dopamine coating membranes showing storage modulus, loss modulus, and tan(δ) vs. temperature.

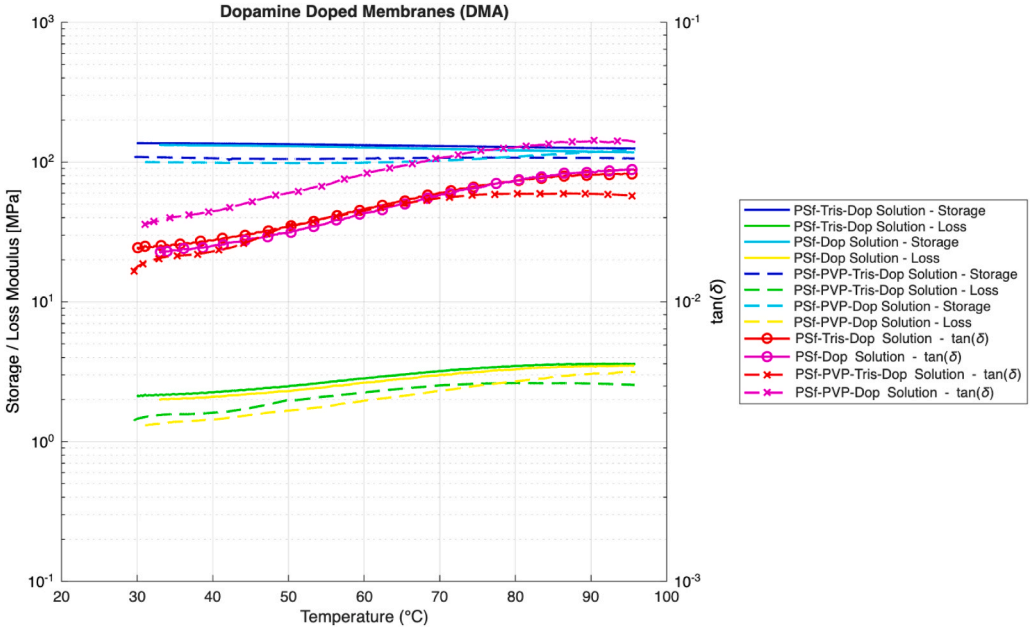

Fig. 10. DMA analysis of dopamine doped solution membranes showing storage modulus, loss modulus, and tan(δ) vs. temperature.

also investigated. In this context, when compared with uncoated PVP-doped membranes, an increase in storage modulus values was observed. Additionally, by comparing the slopes of the curves, it was found that the coating improved the thermal stability of the material's storage modulus. Furthermore, an increase in the loss modulus values was also observed. This indicates that the coating material enhances the energy absorption capability and loss modulus properties of the membrane structure.

The PSf membranes with Tris and Dopamine coating were also studied, and the results are given in Fig. 9. The results obtained from this study indicate that the storage modulus values measured were higher compared to those of other PVP-doped membranes. This is an expected outcome due to the lower porosity of the PSf membrane rather than the PVP-doped membranes. Additionally, compared to the uncoated PSf membrane, the increase in storage modulus values suggests that coating application enhances the membrane's ability to resist applied loads. In the loss modulus results, the values are higher than those of the PSf membrane, and they increase with increasing temperature. However, above 65 °C, the temperature-dependent loss modulus values approach those of the other samples. This indicates that the resistance of the membrane becomes viscous with increasing temperature.

In this study, Tris and Dopamine were applied to the membrane not only as a coating but also as a solution, and manufacturing was carried out accordingly. The temperature-dependent mechanical properties of the solution membranes were determined and presented in this section.

Firstly, the PSf-Tris-Dopamine solution is evaluated, and the results are given in Fig. 10. Examining the obtained graph, a decreasing trend in the storage modulus and an increasing trend in the loss modulus were

observed with increasing temperature. Compared with the PSf membrane, solution treatment was found to increase the storage modulus. Additionally, when compared to the coating application, the solution-treated membrane exhibited a higher storage modulus. Regarding the loss modulus values, the solution-treated sample showed higher loss modulus values.

The case in which only the dopamine solution was applied to the PSf membrane is studied, and the results are given in Fig. 10. A similar trend was observed as with the Tris-containing solution: a decrease in the storage modulus and an increase in the loss modulus with increasing temperature. The obtained storage modulus values were lower at all temperatures compared to the Tris-doped solution. When compared to the PSf membrane, the PSf-Dopamine-solution membrane shows a decreasing storage modulus with temperature, whereas the PSf membrane's storage modulus increases. As a result, the PSf membrane exhibits higher storage modulus values above 87 °C. When examining the loss modulus values, a higher loss modulus is observed compared to the PSf membrane; however, it remains lower than that of the Tris-Dopamine solution and follows a similar downward trend with increasing temperature.

The dopamine and Tris solution were applied to the PSf-PVP membrane, and the mechanical behaviour is given in Fig. 10. An increase in the temperature-dependent loss modulus values was observed, while the slope of the storage modulus curve was close to zero. When comparing mechanical properties with those of the PVP membrane, both the storage and loss modulus values increased with solution treatment. Additionally, a comparison was made with the coated membranes. As a result of this comparison, it was observed that the storage and loss modulus values measured for the coated samples were lower than those of the solution-treated membranes.

The final sample examined was the PSf-PVP-Dopamine solution-treated sample, and the results are given in Fig. 10. Similarly, the storage modulus curve of this sample does not change significantly with temperature, whereas the loss modulus curve shows a slight increase with rising temperature. The storage modulus and loss modulus values measured in the dopamine solution were higher than those in the dopamine and Tris combined solutions after the 80 °C.

3.2.2. Modelling results

Fig. 11 presents the bulk (solid) elastic moduli (E_0) of the membranes recovered from porous DMA measurements using three homogenisation schemes: the Voigt inverse, the Hill inverse, and the self-consistent (SC) inverse model. Across all membrane systems, the recovered bulk values are consistently higher than the directly measured porous counterparts, demonstrating the removal of porosity effects and the estimation of intrinsic polymer stiffness.

The Voigt-inverse estimates yield the lowest values among the three approaches, as the Voigt bound assumes uniform strain and provides an upper bound for composite systems, but, when inverted for porosity correction, results in comparatively lower bulk stiffness. In contrast, the Hill-inverse method, which represents the arithmetic mean of the Voigt and Reuss limits, produces the highest bulk values. This behaviour is expected, as Hill averaging effectively balances uniform stress and strain assumptions, leading to stiffer predictions when porosity is removed. The SC-inverse estimates lie between these extremes, incorporating pore–matrix interactions through a more physically motivated description of spherical voids within an elastic continuum.

The trends across different membrane formulations are broadly consistent: porosity-corrected values converge towards a similar range of intrinsic polymer stiffness, indicating that the bulk polymer matrix dominates the elastic response once porosity is accounted for. Subtle differences between neat, dopamine-doped, and PDA-coated membranes may be linked to changes in polymer-dopant interactions or coating-induced densification; however, the dominant trend highlights that apparent differences in experimental DMA measurements arise primarily from porosity rather than intrinsic material differences.

3.3. Thermal characterisation of membranes

The thermograms obtained from the DSC analyses of the membranes prepared within the scope of this study are presented in Fig. 12. The glass transition temperature (T_g) is commonly used to elucidate the structural characteristics of membranes consisting of a polymer having an amorphous nature (such as polysulfone) [45]. T_g is also a key parameter for evaluating the miscibility of membrane components [46].

PVP is widely known in the literature as an amorphous polymer [47]. It was reported that the T_g of PVP fibres was between 176–183 °C. Moreover, it has been highlighted that above the T_g, the mobility of polymer chains increases significantly [48].

T_g is defined as the midpoint of the specific heat capacity change during the thermal transition [46]. The presence of a single T_g in a DSC thermogram indicates good miscibility of polymers [30] and the absence of another phase transitions [25], while multiple T_g values point out the presence of immiscible phases [46]. Additionally, T_g values can provide insight into membrane morphology. Reduced T_g values generally correspond to a higher fractional free volume, which is associated with a

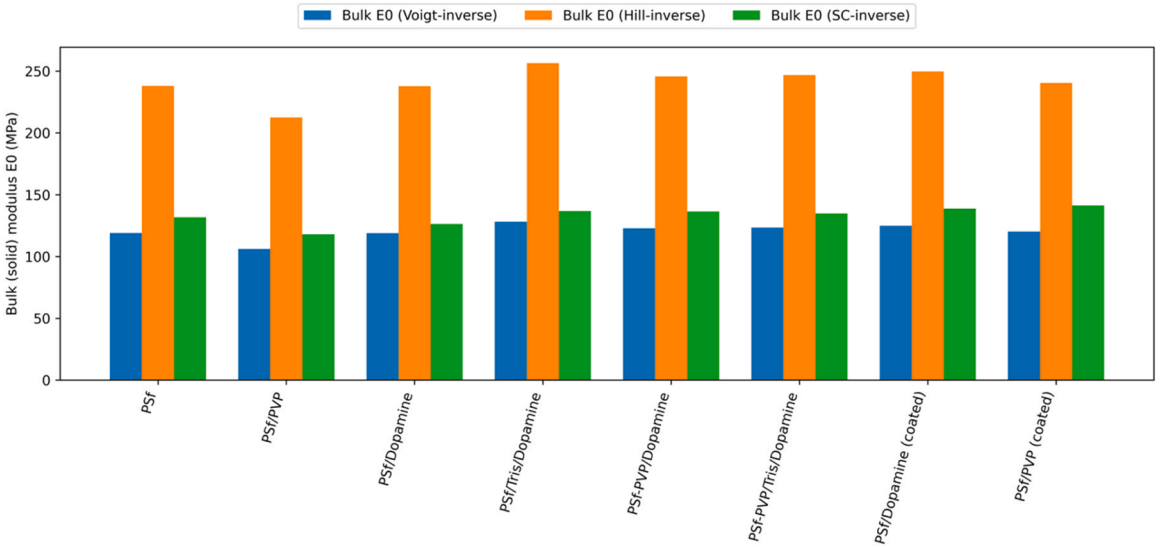

Fig. 11. Bulk (fully dense) elastic moduli, E_0, estimated by inverse homogenisation (Voigt, Hill, and self-consistent) from porous DMA data.

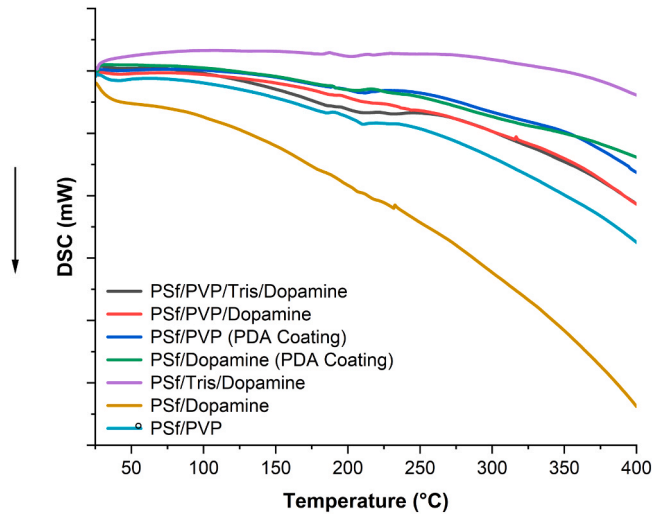

Fig. 12. DSC analysis results.

more loosely packed polymer structure [45]. In general, membranes prepared in our research have a single T_g value, which was attributed to effective miscibility.

As emphasised in previous studies, the addition of PVP to polysulfone [45] and polyethersulfone [48] based membranes reduces T_g values. This was attributed to the variation of flexibility in the chain [46].

In the current study, the T_g values obtained from the DSC thermograms generally fall within the range of 202–223 °C. As mentioned above, the addition of PVP to polysulfone-based membranes has a decreasing effect on T_g values. For example, T_g value decreased from ~215 °C to ~203 °C with the addition of PVP to the membrane composition, which was composed of PSf/Dopamine (PSf/PVP/DOP). Considering the T_g values of PSf/Dopamine and PSf/PVP membranes, it was observed that the use of PVP with PSf reduced the T_g value from 215 °C to 203 °C. Similar results were also obtained for PDA coated membranes. While the Tg value of the PSf/Dopamine (PDA Coating) membrane was determined as 223 °C, the Tg values of the PSf/PVP (PDA Coating) membrane were determined as 202 °C.

On the other hand, it can be stated that the use of Tris in membrane preparation has no significant effect on glass transition temperatures. T_g values of both PSf/Dopamine and PSf/Tris/Dopamine membranes were determined as 215 °C. In PSf/PVP/Dopamine and PSf/PVP/Tris/Dopamine membranes, T_g values decrease with the addition of PVP and are evaluated as 203 °C and 202 °C, respectively, while the effect of Tris on T_g values is negligible.

3.4. Membrane flux performance results

Fig. 13 shows a comparison of the pure water flux, lake water flux, and pure water flux of fouled membranes. The average pure water flux values of the fabricated membranes were calculated. For neat membranes, the average pure water fluxes for PSf and PSf/PVP were 138.9 L/m²·h and 147.95 L/m²·h, respectively. For dopamine-doped membranes (PSf/Dopamine, PSf/Tris/Dopamine, PSf/PVP/Dopamine, PSf/PVP/Tris/Dopamine), the average pure water flux values were determined to be 231 L/m²·h, 266.46 L/m²·h, 324 L/m²·h, and 487.61 L/m²·h, respectively.

For membranes coated with PDA, the average pure water fluxes were 371 L/m²·h for PSf/Dopamine and 395.24 L/m²·h for PSf/PVP. Among all, the PSf/PVP/Tris/Dopamine membrane showed the highest pure water flux value of 487.61 L/m²·h, indicating the best performance. The order of membranes with the highest pure water flux was determined as follows: PSf/PVP/Tris/Dopamine > PSf/PVP Coating > PSf/Dopamine Coating > PSf/PVP/Dopamine > PSf/Tris/Dopamine > PSf/Dopamine

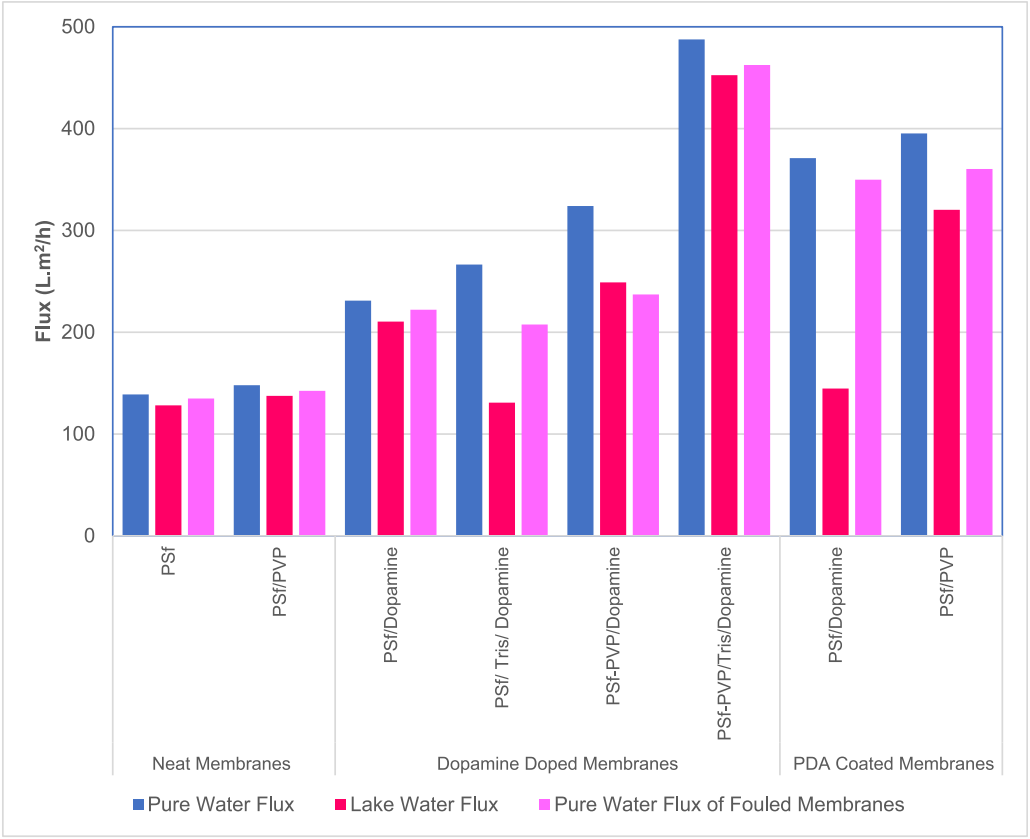

Fig. 13. Pure water flux, lake water flux and pure water flux of fouled membranes.

> PSf/PVP > PSf. From these results, it can be observed in the graphs that the addition of Tris and dopamine increases the membrane flux.

The average lake water flux values of the prepared membranes were also calculated. For neat membranes, the average lake water flux values of PSf and PSf/PVP were 128.19 L/m²·h and 137.5 L/m²·h, respectively. For dopamine-doped membranes (PSf/Dopamine, PSf/Tris/Dopamine, PSf/PVP/Dopamine, PSf/PVP/Tris/Dopamine), the average lake water flux values were 210.42 L/m²·h, 130.81 L/m²·h, 248.98 L/m²·h, and 452.46 L/m²·h, respectively.

For PDA-coated membranes, the average lake water flux values were 144.66 L/m²·h for PSf/Dopamine and 320.26 L/m²·h for PSf/PVP. Again, PSf/PVP/Tris/Dopamine had the highest lake water flux value at 452.46 L/m²·h, making it the best performer in terms of lake water filtration. The ranking of membranes with the highest lake water flux was: PSf/PVP/Tris/Dopamine > PSf/PVP Coating > PSf/PVP/Dopamine > PSf/Dopamine > PSf/Dopamine Coating > PSf/Tris/Dopamine > PSf/PVP > PSf. Again, based on the graphs, it can be concluded that PVP enhances pore formation and that incorporating Tris and dopamine into the membrane structure improves flux performance.

Finally, the average pure water flux values for fouled membranes were calculated. For fouled neat membranes, the average pure water flux values of PSf and PSf/PVP were 134.92 L/m²·h and 142,4 L/m²·h, respectively. For fouled dopamine-doped membranes (PSf/Dopamine, PSf/Tris/Dopamine, PSf/PVP/Dopamine, PSf/PVP/Tris/Dopamine), the average pure water flux values were 222.1 L/m²·h, 207.6 L/m²·h, 237.1 L/m²·h, and 462.44 L/m²·h, respectively.

For fouled PDA-coated membranes, the average pure water flux values were 349.84 L/m²·h for PSf/Dopamine and 360.32 L/m²·h for PSf/PVP. Among these, the fouled PSf/PVP/Tris/Dopamine membrane showed the highest flux value of 462.44 L/m²·h, indicating the best performance. The ranking of fouled membranes in terms of pure water flux was as follows: PSf/PVP/Tris/Dopamine > PSf/PVP Coating > PSf/Dopamine Coating > PSf/PVP/Tris/Dopamine > PSf/Dopamine > PSf/Tris/Dopamine > PSf/PVP > PSf. The flux-enhancing effects of Tris and dopamine, which were prominent in pure and lake water tests, were also retained even after the membranes were fouled, indicating good performance.

The increase in pure water flux observed for the PSf/PVP/Tris/Dopamine membrane can be attributed to the synergistic effects of dopamine-induced hydrophilization and PVP-assisted pore formation. Dopamine/PDA introduces hydrophilic catechol and amine groups, improving water–membrane interactions and permeability [17,49]. Tris buffer enhances dopamine polymerisation efficiency, leading to more effective surface modification [17]. Additionally, PVP contributes to a more open and interconnected substructure, increasing baseline porosity and flux. These well-known mechanisms are consistent with our flux order, while excessive PDA growth may reduce flux through partial pore blockage [35,50].

3.4.1. Comparison of membrane resistance, fouling resistance, and total resistance

Fig. 14 illustrates the resistance values (membrane resistance Rm, fouling resistance Rf, and total resistance Rt) for various membrane types categorised as neat, dopamine-doped, and PDA-coated. For neat membranes (PSf and PSf/PVP), membrane resistance significantly contributes to total resistance with minimal fouling resistance, indicating that intrinsic membrane characteristics dominate rather than fouling phenomena. It is known that PVP is a widely utilised additive in membrane fabrication, and as reported by Wu et al. increasing the PVP content typically enhances the antifouling performance, improves water flux, and forms a hydrophilic layer on the membrane surface, thus offering long-term stability and durability [51].

With dopamine introduction (dopamine-doped membranes), a notable decrease in membrane resistance occurs, but fouling resistance slightly increases, particularly evident in PSf/Tris/Dopamine membranes. Furthermore, PDA-coated membranes, especially PSf/Dopamine, exhibit significantly elevated fouling resistance, indicating that the PDA coating increases membrane affinity to fouling substances, increasing the overall resistance. Therefore, although dopamine generally reduces intrinsic membrane resistance, it also increases susceptibility to fouling, highlighting a trade-off between improved intrinsic resistance and antifouling performance.

3.4.2. Membrane treatment performance results

Fig. 15 presents the manganese removal efficiencies of various membranes when tested with lake water containing an initial

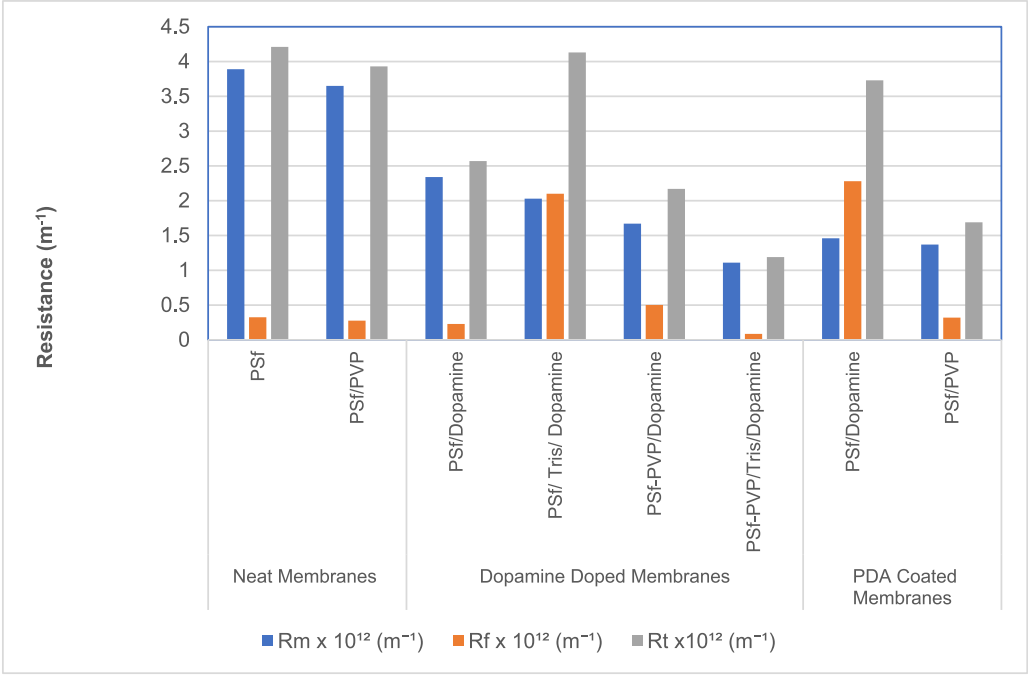

Fig. 14. Comparison of membrane resistance, fouling resistance, and total resistance.

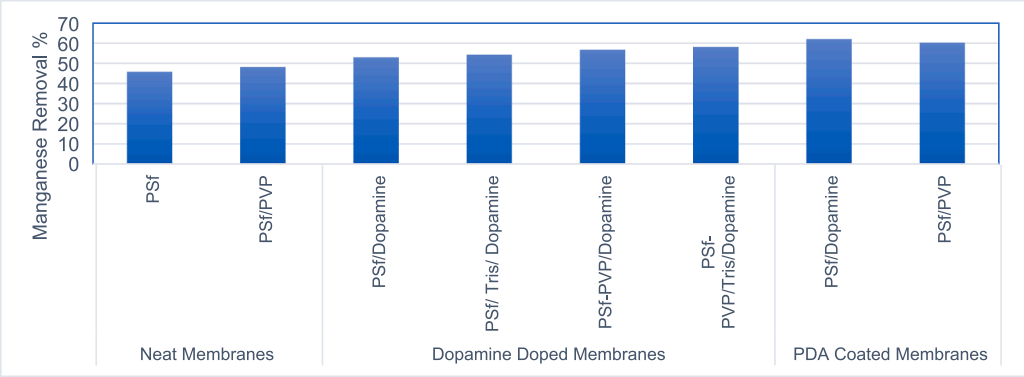

Fig. 15. Manganese removal efficiencies of membranes for lake water.

manganese concentration of 68 μg/L. The removal performances vary significantly depending on the membrane composition and surface modification.

Among all membranes, the highest manganese removal efficiency was observed for the PSf/Dopamine-coated membrane at 62 %, followed closely by the PSf/PVP-coated membrane at 60.3 %. These results highlight the effectiveness of PDA surface coating, which introduces catechol and amine functional groups capable of chelating metal ions such as manganese.

Dopamine- and Tris/dopamine-doped membranes also showed improved manganese removal compared to unmodified membranes. Specifically, PSf/PVP/Tris/Dopamine (58.1 %), PSf/PVP/Dopamine (56.7 %), PSf/Tris/Dopamine (54.3 %), and PSf/Dopamine (53 %) exhibited moderate removal efficiencies. The enhancement in these membranes can be attributed to the presence of dopamine, which contributes to metal-binding capacity through its functional groups.

In contrast, the neat membranes, PSf and PSf/PVP, exhibited the lowest manganese removal efficiencies at 45.8 % and 48.2 %, respectively. These values suggest that membranes without functional modification have limited interaction with manganese ions and are thus less effective at removing them from lake water.

The superior manganese removal observed with PDA-coated membranes, such as PSf/Dopamine-coated membranes, can be attributed to the surface-bound catechol and amine groups provided by the PDA coating, which offer highly accessible and abundant metal-binding sites directly on the membrane surface. In contrast, dopamine doping likely disperses these functional groups more diffusely within the membrane matrix, resulting in fewer accessible sites for manganese binding at the membrane-water interface. This spatial distribution difference significantly impacts the efficiency of metal ion chelation, explaining why PDA coatings outperform dopamine doping.

Moreover, while increased hydrophilicity of the membrane surface improves water permeation and general fouling resistance, it is important to clarify that hydrophilicity alone does not ensure affinity toward manganese ions. The specific interactions between catechol and amine functional groups, as opposed to general hydrophilic groups such as hydroxyl (–OH) groups, are essential for forming strong coordination complexes with Mn^{2+} ions. Therefore, the observed enhancements in manganese removal performance are primarily due to these specialised ligand interactions, which are more effectively presented through surface-bound PDA coatings.

Overall, the data indicate that PDA coating provides the highest manganese removal, while dopamine and Tris/dopamine doping also significantly enhance performance. These improvements are likely due to increased surface hydrophilicity and the availability of functional groups that increase metal ion binding. Therefore, surface modification strategies, particularly PDA coating, are effective approaches for improving the metal ion removal performance of polymeric membranes.

4. Conclusions

In this study, polysulfone (PSf)-based ultrafiltration membranes were fabricated and systematically modified using dopamine sourced from mussels via functionalisation and polydopamine (PDA) coating, with additional contributions from polyvinylpyrrolidone (PVP) and tris (hydroxymethyl)aminomethane (Tris). These components were deliberately selected to enhance porosity, promote dopamine polymerisation, and improve both mechanical and filtration properties. The fabrication strategy yielded a diverse set of membranes, enabling the combined effects of PVP-induced porosity and dopamine-related modifications on structure, mechanics, and performance to be comprehensively assessed.

Structural and physicochemical characterisation demonstrated that the modifications induced clear and complementary changes in the membrane architecture. SEM confirmed the enhancement of pore size and distribution with PVP, while FTIR validated the presence of dopamine and PDA functional groups on the membrane surface. Contact angle analysis indicated a marked reduction in hydrophobicity due to dopamine functionalisation. XRD analysis showed that the crystalline features of PSf were preserved after modification, but also suggested subtle structural interactions between the polymer matrix and the introduced additives. These results collectively verified that the fabrication strategy successfully combined increased porosity with improved surface chemistry.

The thermo-mechanical behaviour of the membranes was investigated using DSC and DMA. DSC confirmed the thermal stability of the polymeric membranes, with minor shifts indicating the influence of additives on the glass transition behaviour. DMA provided detailed storage modulus values, which were then integrated with micromechanical modelling to separate the apparent stiffness of porous membranes from the intrinsic stiffness of the dense polymer. While the Voigt and Reuss models provided upper and lower bounds, the Hill average offered an intermediate reference. The self-consistent scheme, however, was most effective at capturing the reduction in stiffness caused by porosity, yielding the closest agreement with experimental values. Through this approach, the effective moduli of the polymer matrix were recovered, providing a more accurate representation of the material's mechanical properties.

Filtration performance testing established a clear link between structural and thermo-mechanical modifications and water treatment efficiency. The PSf/PVP/Tris/Dopamine-doped membrane achieved the highest pure water flux, and maintained a high flux with lake water. PDA-coated membranes, while exhibiting slightly lower flux than the PVP/Tris/Dopamine-doped variants, demonstrated superior mechanical robustness, confirming the reinforcing effect of surface PDA layers. Dopamine-modified membranes achieved the highest Mn(II) removal efficiency, but also displayed greater susceptibility to fouling-induced flux decline. These findings highlight the trade-off between maximising hydrophilicity and maintaining fouling resistance, emphasising

the importance of balancing surface chemistry with mechanical stability in practical applications.

Taken together, this study demonstrates that dopamine, a naturally derived compound from mussel adhesion proteins, can serve as a sustainable, multifunctional modifier for polymeric membranes. By combining dopamine functionalisation with porosity-enhancing additives such as PVP and Tris, it is possible to simultaneously improve structural, thermo-mechanical, and filtration properties. The integration of micromechanical modelling with experimental characterisation further strengthens the analysis, allowing the intrinsic polymer stiffness to be distinguished from porosity effects. This comprehensive framework not only establishes the benefits of dopamine- and PDA-functionalised membranes for enhanced water purification but also underscores their role as environmentally conscious alternatives in the development of next-generation filtration technologies.

Funding

This research is funded by Istanbul University-Cerrahpasa Scientific Research Projects Coordination Unit, grant number FYL-2024–37538.

CRediT authorship contribution statement

Neşe Tüfekci: Writing – review & editing, Writing – original draft, Visualization, Validation, Supervision, Software, Resources, Project administration, Methodology, Investigation, Funding acquisition, Formal analysis, Conceptualization. **Selva Çavuş:** Writing – original draft, Validation, Resources, Methodology, Investigation, Funding acquisition, Formal analysis, Conceptualization. **Sevgi Güneş Durak:** Writing – review & editing, Writing – original draft, Visualization, Validation, Resources, Methodology, Investigation, Formal analysis. **Mertol Tüfekci:** Writing – review & editing, Writing – original draft, Software, Resources, Methodology, Investigation, Formal analysis, Conceptualization. **Sağra Sağlam:** Writing – original draft, Visualization, Validation, Resources, Methodology, Investigation, Formal analysis. **İnci Pir:** Writing – original draft, Validation, Software, Methodology, Investigation, Formal analysis, Conceptualization. **Kawthr Rukiah:** Writing – review & editing, Writing – original draft, Visualization, Validation, Methodology, Investigation, Funding acquisition, Formal analysis. **Güler Türkoğlu Demirkol:** Supervision, Resources, Project administration, Methodology, Investigation, Funding acquisition, Formal analysis, Conceptualization.

Declaration of Competing Interest

The authors declare that they have no known competing financial interests or personal relationships that could have appeared to influence the work reported in this paper.

Acknowledgement

The authors gratefully acknowledge Türkan Ormancı Acar for her valuable contributions and insightful guidance, generously sharing her professional experience and expertise throughout this study. Also, the authors would like to thank Şevval Zenler for her support in the visualisation of some figures used in this manuscript.

Data availability

No data was used for the research described in the article.

References

[1] S. Güneş-Durak, S. Acarer-Arat, M. Tüfekci, İ. Pir, Z. Üstkaya, N. Öz, N. Tüfekci, Mechanical enhancement and water treatment efficiency of nanocomposite PES membranes: a study on Akçay dam water filtration application, ACS Omega 9 (2024) 31556–31568.
[2] Acarer-Arat S., Pir İ, Tüfekci M., Güneş-Durak S., Akman A. and Tüfekci N. 2024 Heavy metal rejection performance and mechanical performance of cellulose-nanofibril-reinforced cellulose acetate membranes ACS Omega.
[3] S. Acarer-Arat, M. Tüfekci, İ. Pir, N. Tüfekci, Nanocellulose in polyvinylidene fluoride (PVDF) membranes: assessing reinforcement impact and modelling techniques, J. Environ. Chem. Eng. 12 (2024) 114749.
[4] P.B. Messersmith, Multitasking in tissues and materials, Science (1979) (2008) 319.
[5] N.F. Della Vecchia, A. Luchini, A. Napolitano, G. Derrico, G. Vitiello, N. Szekely, M. Dischia, L. Paduano, Tris buffer modulates polydopamine growth, aggregation, and paramagnetic properties, Langmuir 30 (2014) 9811–9818.
[6] J. Yang, L. Niu, Z. Zhang, J. Zhao, L. Chou, Electrochemical behavior of a polydopamine nanofilm, Anal. Lett. 48 (2015) 2031–2039.
[7] S. Sharma, D. Mudgal, V. Gupta, Polydopamine coating on additive manufacturing-based poly lactic acid structures with controllable parameters for enhanced mechanical properties: an experimental investigation, Polym. Eng. Sci. 62 (2022) 3523–3542.
[8] R. Shevate, M. Kumar, M. Karunakaran, M.N. Hedhili, K.V. Peinemann, Polydopamine/Cysteine surface modified isoporous membranes with self-cleaning properties, J. Memb. Sci. 529 (2017) 185–194.
[9] S. Rudzinski, L. Häussler, C.H. Harnisch, E. Mäder, G. Heinrich, Glass fibre reinforced polyamide composites: thermal behaviour of sizings, Compos Part A Appl. Sci. Manuf. 42 (2011).
[10] Y.M. Shin, I. Jun, Y.M. Lim, T. Rhim, H. Shin, Bio-inspired immobilization of cell-adhesive ligands on electrospun nanofibrous patches for cell delivery, Macromol. Mater. Eng. 298 (2013) 555–564.
[11] S. Muchtar, M. Wahab, S. Mulyati, M. Riza, N. Arahman, Deposition of polydopamine on the surface of polyvinylidene fluoride (PVDF) membrane as a UV-shielding layer, IOP Conf. Ser. Mater. Sci. Eng. 523 (2019) 012017.
[12] Z.H. Chang, L.H.T. Lyly, Y.H. Teow, S.P. Yeap, J.Y. Sum, Insight into polydopamine coating on microfiltration membrane with controlled surface pore size for enhanced membrane rejection, Polymers 287 (2023) 126446.
[13] N. Alshammari, M. Alazmi, V.N. Veettil, Applying a hydrophilic modified hollow fiber membrane to reduce fouling in artificial lungs, Separations 8 (2021). *Page 113* **8** 113.
[14] S. Kasemset, Z. He, D.J. Miller, B.D. Freeman, M.M. Sharma, Effect of polydopamine deposition conditions on polysulfone ultrafiltration membrane properties and threshold flux during oil/water emulsion filtration, Polymers 97 (2016) 247–257.
[15] F. Altaf, S. Ahmed, M. Usman, T. Batool, J. Shamshad, P. Bocchetta, R. Batool, Removal of heavy metals from wastewater using novel polydopamine-modified CNTs-based composite membranes, Processes 9 (2021). *Page 2120* **9** 2120.
[16] F. Marpani, J. Luo, R.V. Mateiu, A.S. Meyer, M. Pinelo, In situ formation of a biocatalytic alginate membrane by enhanced concentration polarization, ACS Appl. Mater. Interfaces 7 (2015) 17682–17691.
[17] S. Mulyati, S. Muchtar, N. Arahman, Y. Syamsuddin, N.I. Mat Nawi, N. Yub Harun, M.R. Bilad, Y. Firdaus, R. Takagi, H. Matsuyama, Two-step dopamine-to-polydopamine modification of polyethersulfone ultrafiltration membrane for enhancing anti-fouling and ultraviolet resistant properties, Polymers 12 (2020) 2051.
[18] J. Feng, Z. Guo, Effects of temperature and frequency on dynamic mechanical properties of glass/epoxy composites, J. Mater. Sci. 51 (2016).
[19] ASTM 2015 Test Method for Glass Transition Temperature (DMA Tg) of Polymer Matrix Composites by Dynamic Mechanical Analysis (DMA).
[20] F. Altaf, R. Gill, R. Batool, Zohaib-Ur-Rehman, H. Majeed, G. Abbas, K. Jacob, Synthesis and applicability study of novel poly(dopamine)-modified carbon nanotubes based polymer electrolyte membranes for direct methanol fuel cell, J. Environ. Chem. Eng. 8 (2020) 104118.
[21] X. Geng, J. Wang, J. Ye, S. Yang, Q. Han, H. Lin, F. Liu, Electrosprayed polydopamine membrane: Surface morphology, chemical stability and separation performance study, Sep Purif. Technol. 244 (2020) 116857.
[22] İ.S. Üçel, E. Demirel, Modification of PVDF membranes using dopamine/zinc oxide for lead removal from aqueous media, Open J. Nano 7 (2022) 53–73.
[23] E. Eren, A. Sarihan, B. Eren, H. Gumus, F.O. Kocak, Preparation, characterization and performance enhancement of polysulfone ultrafiltration membrane using PBI as hydrophilic modifier, J. Memb. Sci. 475 (2015) 1–8.
[24] Z. Liu, Z. Mi, C. Chen, H. Zhou, X. Zhao, D. Wang, Preparation of hydrophilic and antifouling polysulfone ultrafiltration membrane derived from phenolphthalin by copolymerization method, Appl. Surf. Sci. 401 (2017) 69–78.
[25] X. Wu, Z. Xie, H. Wang, C. Zhao, D. Ng, K. Zhang, Improved filtration performance and antifouling properties of polyethersulfone ultrafiltration membranes by blending with carboxylic acid functionalized polysulfone, RSC Adv. 8 (2018) 7774–7784.
[26] E. Vázquez, C. Muro, J. Illescas, G. Burillo, O. Hernández, E. Rivera, Obtainment and characterization of hydrophilic polysulfone membranes by N-vinylimidazole grafting induced by gamma irradiation, Polymers 12 (2020). *Page 1284* **12** 1284.
[27] A. Febriasari, Huriya, A.H. Ananto, M. Suhartini, S. Kartohardjono, Polysulfone–polyvinyl pyrrolidone blend polymer composite membranes for batik industrial wastewater treatment, Membranes 2021 11 (2021). *Page 66* **11** 66.
[28] J. Chokki, G. Darracq, P. Poelt, J. Baron, H. Gallard, M. Joyeux, B. Teychené, Investigation of Poly(ethersulfone)/Polyvinylpyrrolidone ultrafiltration membrane degradation by contact with sodium hypochlorite through FTIR mapping and two-dimensional correlation spectroscopy, Polym. Degrad. Stab. 161 (2019) 131–138.
[29] W.A.W. Rafizah, A.F. Ismail, Effect of carbon molecular sieve sizing with poly(vinyl pyrrolidone) K-15 on carbon molecular sieve–polysulfone mixed matrix membrane, J. Memb. Sci. 307 (2008) 53–61.

[30] M. Zahid, A. Rashid, S. Akram, Z.A. Rehan, W. Razzaq, A comprehensive review on polymeric nano-composite membranes for water treatment, J. Membr. Sci. Technol. 08 (2018).
[31] Y. Alqaheem, A.A. Alomair, Microscopy and spectroscopy techniques for characterization of polymeric membranes, Membranes 10 (2020). *Page 33* **10** 33.
[32] S.T. Muntha, M. Siddiq, A. Kausar, A. Khan, Mixed matrix membranes of polysulfone/polyimide reinforced with modified zeolite based filler: preparation, properties and application, Chin. J. Polym. Sci. (English Edition) 36 (2018) 65–77.
[33] P.F. Andrade, A.F. de Faria, S.R. Oliveira, M.A.Z. Arruda, M. do C. Gonçalves, Improved antibacterial activity of nanofiltration polysulfone membranes modified with silver nanoparticles, Water Res. 81 (2015) 333–342.
[34] T. Bucher, J. Clodt, A. Grabowski, M. Hein, V. Filiz, Colour-value based method for polydopamine coating-stability characterization on polyethersulfone membranes, Membranes 7 (2017) 70.
[35] S. Kasemset, L. Wang, Z. He, D.J. Miller, A. Kirschner, B.D. Freeman, M.M. Sharma, Influence of polydopamine deposition conditions on hydraulic permeability, sieving coefficients, pore size and pore size distribution for a polysulfone ultrafiltration membrane, J. Memb. Sci. 522 (2017) 100–115.
[36] J.S. Hsu, B.J. Wen, L.J. Chang, Thermal property measurement of polymer materials, Adv. Mat. Res. 591–593 (2012) 1089–1093.
[37] T. Jin, C.W. Coley, A. Alexander-Katz, Molecular signatures of the glass transition in polymers, Phys. Rev. E 106 (2022) 014506.
[38] K. Hickey, J. Feinstein, G. Sivaraman, M. MacDonell, E. Yan, C. Matherson, S. Coia, J. Xu, K. Picel, Applying machine learning and quantum chemistry to predict the glass transition temperatures of polymers, Comput. Mater. Sci. 238 (2024) 112933.
[39] V. Dogra, A. Gaur, C. Kishore, A. Verma, Effect of reinforcement materials on the glass transient temperature and viscoelastic properties of polymer composites. Dynamic Mechanical and Creep-Recovery Behavior of Polymer-Based Composites, Elsevier, 2024, pp. 189–202.
[40] C. Liu, H. Mao, J. Zheng, S. Zhang, Tight ultrafiltration membrane: Preparation and characterization of thermally resistant carboxylated cardo poly (arylene ether ketone)s (PAEK-COOH) tight ultrafiltration membrane for dye removal, J. Memb. Sci. 530 (2017) 1–10.
[41] A. Kausar, M. Siddiq, Nanofiltration membranes of poly(styrene-co-chloro-methylstyrene)-grafted-DGEBA reinforced with gold and polystyrene nanoparticles for water purification, Appl. Water Sci. 7 (2017) 1323–1335.
[42] H.L. Ornaghi, L.K. Lazzari, E.F. Kerche, R.M. Neves, Dynamic mechanical behavior of polymer, Nanocomposites (2023) 147–161.
[43] N. Saba, M. Jawaid, O.Y. Alothman, M.T. Paridah, A review on dynamic mechanical properties of natural fibre reinforced polymer composites, Constr. Build. Mater. 106 (2016) 149–159.
[44] K.P. Menard, N.R. Menard, Dynamic Mechanical Analysis, CRC Press, 2020.
[45] G.D. Vilakati, A.S. Mtsetfwa, L.D. Mafu, G. Mamba, D.S. Dlamini, M.M. Motsa, Probing the separation efficiency of sulfur-doped graphitic carbon nitride (g-C3N4)/polysulfone low-pressure ultrafiltration mixed matrix membranes, Polym. Bull. 80 (2023).
[46] N. Bolong, A.F. Ismail, M.R. Salim, D. Rana, T. Matsuura, Development and characterization of novel charged surface modification macromolecule to polyethersulfone hollow fiber membrane with polyvinylpyrrolidone and water, J. Memb. Sci. 331 (2009) 40–49.
[47] A.L. Saroj, R.K. Singh, S. Chandra, Studies on polymer electrolyte poly(vinyl) pyrrolidone (PVP) complexed with ionic liquid: effect of complexation on thermal stability, conductivity and relaxation behaviour, Mater. Sci. Eng. B 178 (2013) 231–238.
[48] O. Elishav, V. Beilin, O. Rozent, G.E. Shter, G.S. Grader, Thermal shrinkage of electrospun PVP nanofibers, J. Polym. Sci. B Polym. Phys. 56 (2018) 248–254.
[49] N. Abounahia, H. Qiblawey, S.J. Zaidi, Progress for co-incorporation of polydopamine and nanoparticles for improving membranes performance, Membranes 12 (2022) 675.
[50] A. Cihanoğlu, J.D. Schiffman, S. Alsoy Altinkaya, Biofouling-resistant ultrafiltration membranes via codeposition of dopamine and cetyltrimethylammonium bromide with retained size selectivity and water flux, ACS Appl. Mater. Interfaces 14 (2022) 38116–38131.
[51] Y. Wu, J. Zeng, Y. Zeng, H. Zhou, G. Liu, J. Jian, J. Ding, Polyethersulfone-polyvinylpyrrolidone composite membranes: effects of polyvinylpyrrolidone content and polydopamine coating on membrane morphology, structure and performances, Chin. J. Chem. Eng. 38 (2021) 84–97.